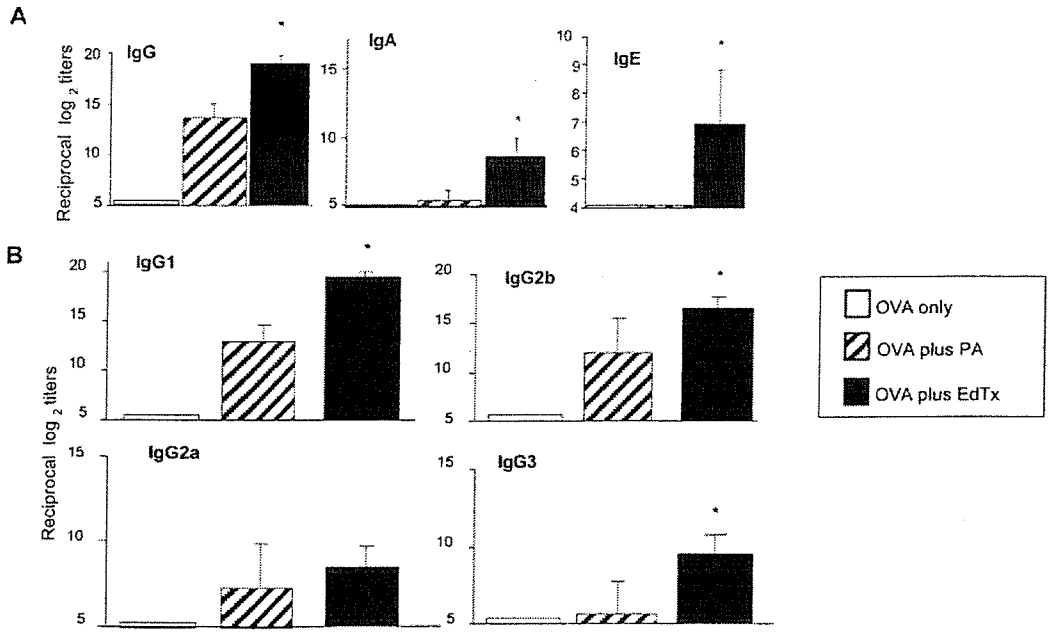

FIGURE 2. Plasma PA-specific Ab responses following nasal immunization with EdTx as adjuvant. Mice were immunized three times at weekly intervals with 100 μg of OVA only (□), OVA plus 5 μg of PA (▨), or OVA plus 5 μg of EdTx (5 μg of PA plus 5 μg of EF) (■). Plasma PA-specific IgE Ab responses were determined in samples collected at day 14, and plasma PA-specific Ab isotype (*A*) and IgG subclass responses (*B*) were determined 1 wk after the last immunization. The results are expressed as the reciprocal $\log_2$ titer ± one SD from five separate experiments and four mice per group per experiment. *, $p < 0.05$

OVA and EdTx contained significant levels of anti-PA neutralizing Abs (Table I). No significant neutralizing Abs were detected in vaginal washes (Table I).

Ag-specific T cell cytokine responses following nasal immunization with EdTx as adjuvant

To characterize $CD4^+$ Th cell cytokine pathways associated with EdTx-induced immunity, we examined the pattern of cytokines secreted by OVA- and PA-specific $CD4^+$ T cell after a 5-day in vitro restimulation. Spleen $CD4^+$ T cells from mice immunized with OVA and EdTx secreted mixed Th1- and Th2-type cytokines after in vitro restimulation with OVA or PA as indicated by high levels of IFN-γ (Th1) but also IL-5, IL-6, and IL-13 in culture supernatants (Table II). IL-4 levels were below the limit of detection. The same profile of cytokine responses was seen in the culture supernatant of CLN $CD4^+$ T cells restimulated under the same conditions (data not shown).

Effect of EdTx on cytokine secretion and costimulatory molecule expression by Mϕ, in vitro

We assessed the direct effects of EdTx or CT on the expression of costimulatory molecules (i.e., CD40 and CD86) as well as cytokine secretion by J774 Mϕ to address whether EdTx regulates APC functions. Consistent with previous reports (44–46), CT induced high levels of IL-6 responses in treated cells (Fig. 4*A*) and increased costimulatory molecule expression (Fig. 4*B*) by Mϕ in vitro. The IL-6 responses after EdTx stimulation were ~10-fold lower than those measured in culture supernatants of J774 Mϕ cultured in the presence of CT (Fig. 4). However, EdTx up-regulated the expression of both CD40 and CD86 by J774 Mϕ to the same extent as the mucosal adjuvant CT. These findings were further confirmed on T cell-depleted spleen cells (data not shown).

Nasal PA does not target CNS tissues

We next explored the possibility that EdTx could target the ON/E or other CNS tissues and induce inflammatory responses. Fig. 5*A*

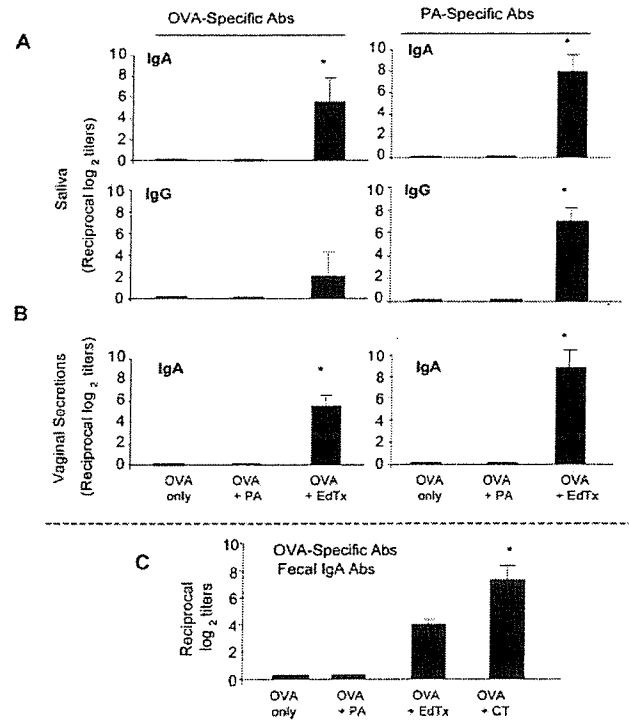

FIGURE 3. Mucosal IgA Ab responses following nasal immunization with EdTx as adjuvant. Mice were immunized three times at weekly intervals with 100 μg of OVA only, OVA plus 5 μg of PA, or OVA plus 5 μg of EdTx (5 μg of PA plus 5 μg of EF). Saliva (*A*) and vaginal washes (*B*) were collected 2 wk after the last immunization. The Ab levels are expressed as the reciprocal $\log_2$ titer ± 1 SD from five separate experiments and four mice per group per experiment. Fecal extracts (*C*) were collected 2 wk after the last immunization with either OVA only, OVA plus PA, OVA plus EdTx, or OVA plus CT. The IgA Ab levels were expressed as the reciprocal $\log_2$ titer ± 1 SD from three separate experiments and four mice per group per experiment. *, $p < 0.05$

Table I. *Neutralizing anti-PA Abs produced in response to nasal administration of EdTx protect Mϕ against the lethal effect of LeTx in vitro*[a]

Immunization	Neutralizing Ab Titers (1/Dilution)		
	Plasma	Saliva	Vaginal Washes
OVA only	BD	BD	BD
OVA plus PA	8,192 ± 256*	BD	BD
OVA plus EdTx	131,072 ± 1,024*	10 ± 3*	3 ± 2

[a] Serial dilutions of each sample were added to J774 Mϕ cultures in the presence of LeTx. The neutralizing titers were determined as the last dilution yielding an MTT OD equal to twice the background value. Results are shown as neutralizing Ab titers and are expressed as the reciprocal dilutions titers ± 1 SE of three separate experiments and five mice per group per experiment. BD, Below detection level; *, $p < 0.05$.

illustrates the failure of PA to accumulate in the ON/E 24 h following nasal delivery of 5 μg of PA. In addition, there was no PA detectable in the OBs or brain and only minor amounts (< 0.15 ng/10 mg tissue) were observed in the NALT, CLN, or spleen 24 h after nasal delivery (data not shown). Nasal PA given together with EF (EdTx) did not increase PA accumulation in olfactory or brain tissues (Fig. 5*A*). In contrast to PA or EdTx, nasal delivery of a 0.5-μg dose of CT resulted in significant accumulation in the ON/E which was further increased when the CT dose was 10-fold higher (Fig. 5*A*). We also found that nasal CT, but not EdTx, up-regulated IL-1 mRNA levels in the ON/E and in the NALT suggesting that CT targeted these two sites (Fig. 5*B*). Finally, mice given nasal CT, but not those given nasal EdTx, exhibited high levels of IL-6 in nasal washes (Fig. 5*C*).

Discussion

The enterotoxins CT and LT-1, which deliver their ADP ribosyl transferase A subunit via ganglioside targeting, are well-recognized adjuvants for induction of mucosal immunity to coadministered Ags (40–42). The CTA1-DD molecule which targets CT-A to B cells was also shown to be an effective mucosal adjuvant (31, 47, 48). EdTx delivers its adenylate cyclase EF subunit into target cells following binding of PA on its membrane receptors, the ATRs. It has been recently reported that ATR1/TEM8 is expressed by epithelial cells (49). However, previous studies have shown that PA binds more effectively to the basolateral membrane of polarized epithelial cells (50), suggesting that ATRs may not be expressed at the apical membrane of these cells. In this study, we show that EdTx promotes both systemic and mucosal adaptive immunity to nasally coadministered Ags and enhances PA-specific Ab responses significantly above levels achieved by administration of PA without EF. We also show that ATR targeting by EdTx did not lead to the accumulation of this adjuvant into olfactory and CNS tissues.

Anthrax toxin derivatives have been evaluated as molecular syringes for intracellular delivery of peptides (13, 51) or protein Ags (14–16) for presentation via the MHC class I pathway and induction of cytotoxic $CD8^+$ T cells. Our results show that in vivo delivery of anthrax EdTx provides necessary signals for induction of mucosal and systemic immunity to coadministered protein Ags. Although data summarized in this manuscript only referred to nasal delivery of EdTx, we also found that EdTx is an adjuvant for protein Ags coinjected i.p. in both C57BL/6 and BALB/c mice (data not shown). Studies with the ganglioside-targeting enterotoxins CT and LT-I (52–55) and derivatives including their chimeras (34, 56) or the B cell-targeting CTA1-DD (31, 57) have demonstrated the importance of receptor binding for controlling the immune responses induced by these ADP-ribosylating adjuvants. Thus, the adjuvant activity of CT appears to be more dependent on IL-4 and $CD4^+$ Th2 cell cytokines (52, 53). In contrast, the more promiscuous LT-I, which binds GM1 gangliosides like CT but also asialo-GM1 and -GM2 gangliosides, promotes a broader spectrum of responses with $CD4^+$ Th cells producing both IFN-γ and Th2-type cytokines (34, 54). The adjuvant activity of nasal EdTx appears to involve Ab and T cells responses that resemble those induced by LT-I rather than CT. Thus, EdTx induced $CD4^+$ T cells secreting both IFN-γ and Th2-type cytokines. Further, EdTx as an adjuvant promoted only modest levels of OVA-specific IgE ($\log_2$ titers = 3) when compared with those seen after nasal immunization with CT (i.e., $\log_2$ titers = 8). Although it has been suggested that ATRs may not be expressed at the apical membrane of epithelial cells (50), there is no information to date on the relative expression of ATRs on immune cells and potential cellular targets of nasally administered EdTx. We have shown here that PA alone or as a component of EdTx does not target olfactory tissues and do not induce IL-1-specific mRNA in ON/E. It is also important to note that EdTx promotes a similar profile of serum Ab responses than CTA1-DD which targets B cells (31).

The mechanisms underlying the induction of mucosal immunity and S-IgA Ab responses by bacterial toxins remain only partially understood. Studies over the past two decades have shown a role for CT-induced cytokines on its mucosal adjuvanticity. Thus, CT was shown to induce both IL-6 and IL-1 secretion by epithelial cells and APCs (44, 58–60). Both IL-1 and IL-6 were later shown to be adjuvants for systemic immunity to nasally coadministered protein vaccines (38, 61) and IL-1 was also able to promote mucosal IgA Ab responses (61). Other factors thought to contribute to the adjuvanticity of CT include its ability to up-regulate the expression of MHC (44) and costimulatory molecules (45, 46, 62).

Table II. *Ag-specific $CD4^+$ T cell cytokine responses induced by nasal EdTx as an adjuvant*[a]

Immunization	In vitro Stimulation	Cytokines (pg/ml)			
		IFN-γ	IL-5	IL-6	IL-13
OVA only	None	156 ± 30	BD	36 ± 1	20 ± 2
	OVA	1320 ± 49*	41 ± 1*	175 ± 10*	36 ± 6
	PA	189 ± 10	BD	31 ± 1	20 ± 0
OVA plus EdTx	None	267 ± 37	BD	31 ± 1	20 ± 0
	OVA	9666 ± 1524*	418 ± 85*	386 ± 16*	188 ± 29*
	PA	16550 ± 2557*	1340 ± 160*	192 ± 28*	406 ± 78*

[a] Spleen $CD4^+$ T cells were isolated 21 days after the initial immunization and restimulated in vitro with OVA (1 mg/ml) or PA (20 μg/ml). Culture supernatants were collected after 5 days and cytokines evaluated by ELISA. The results are expressed as the mean ± 1 SE and are representative of four separate experiments. The same profile of responses was seen with $CD4^+$ T cells isolated from corresponding cervical lymph nodes. BD, Below detection levels; *, $p < 0.05$

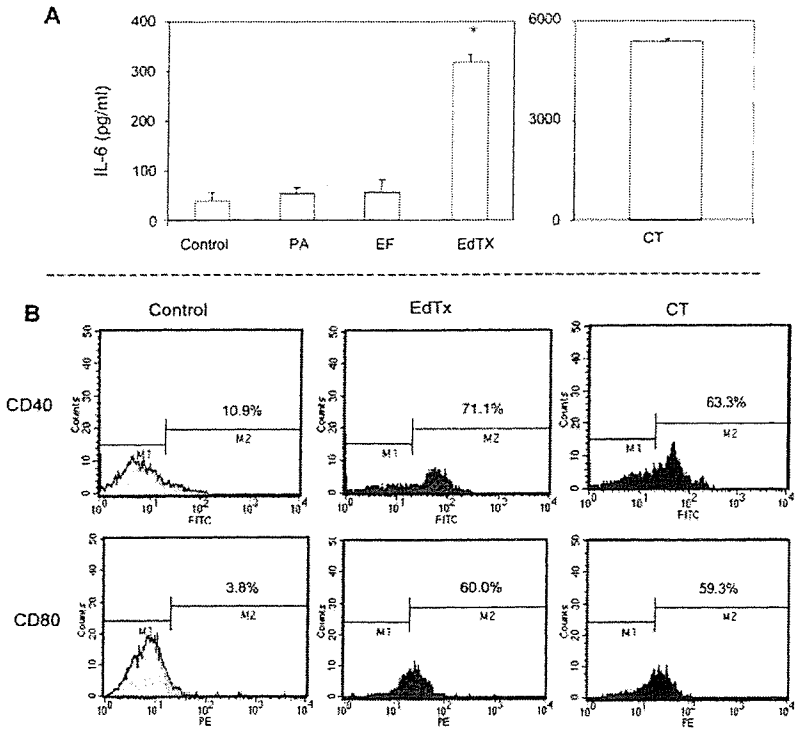

FIGURE 4. Effects of EdTx on cytokine secretion and costimulatory molecule expression by Mϕ. The J774 Mϕ were cultured for 48 h in the presence of PA (5 μg/ml), EF (5 μg/ml), EdTx (5 μg/ml PA + 5 μg/ml EF), or CT (1 μg/ml). *A*, Cytokine secretion was analyzed in culture supernatants, and results were expressed as mean $\pm$ 1 SD of four separate experiments (*, $p < 0.05$). *B*, Cells were analyzed by flow cytometry for expression CD40 and CD86. Results are representative of four separate experiments.

We have shown that EdTx stimulates IL-6 secretion by Mϕ cultures and enhances the expression of costimulatory molecules. We should stress that IL-6 levels induced by EdTx were ~10-fold lower than those seen in Mϕ cultures stimulated with the same dose of CT. The lower stimulatory effect of EdTx for IL-6 secretion was further confirmed in vivo where nasal delivery of CT but not EdTx induced IL-6 secretion in nasal washes. It is unlikely that the reduced ability of EdTx to induce IL-6 (and IL-1) could alone explain the polarized Ag-specific mucosal IgA Abs responses when compared with those generally induced by CT (34, 46, 63) or LT as adjuvants (34, 46, 54, 56). The role of the adenylate cyclase activity for the adjuvanticity remains to be elucidated. In this regard, the EF used in our studies contains a S447N mutation that could account for its recently reported 20-fold lower ability to

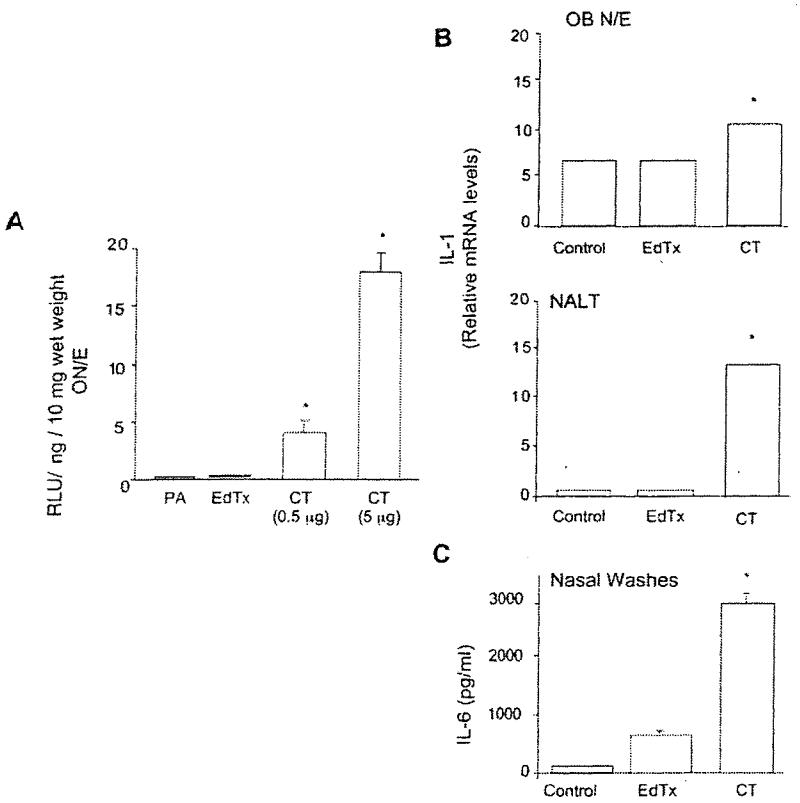

FIGURE 5. *A*, Tracking uptake into olfactory and CNS tissues. Groups of mice were given acridinium-labeled PA (5 μg), EdTx (5 μg of PA plus 5 μg of EF), or CT (0.5 or 5 μg) by the nasal route. *A*, Twenty-four hours later, mice were sacrificed and the ON/E and OBs were collected, homogenized, and tested for light activity as described in *Materials and Methods*. Results are expressed as mean RLU per nanogram of individual tissues $\pm$ 1 SD and are from two separate experiments with three mice per group (*, $p < 0.05$). *B*, IL-1 mRNA analysis by real-time RT-PCR. Results are expressed as mean relative mRNA levels from triplicate assays performed with pooled tissues (three mice per group) and are representative of three separate experiments (*, $p < 0.05$). *C*, Analysis of IL- 6 levels in nasal washes by ELISA. Results are expressed as picograms per milliliter $\pm$ 1 SD of IL-6 levels in individual nasal washes and are from two experiments with three mice per group. *, $p < 0.05$ when compared with controls given PBS.

induce cAMP when compared with recombinant native EF protein (33). Several mutants of both CT and LT-I, which are devoid of ADP-ribosyl transferase activity, were shown to retain their mucosal adjuvant activity and the ability to promote high mucosal IgA Ab responses. In another system, the mucosal adjuvant activity of CTA1-DD was reported to require both effective B cell targeting and the ADP ribosyl transferase activity (57). Thus, further studies are warranted to establish the mechanisms of mucosal adjuvanticity of EdTx.

Enterotoxin adjuvants are also potent immunogens which induce elevated immune responses to their binding subunits (41, 43). A major finding of this study resides in the fact that EdTx is a potent immunogen and that the presence of EF increased anti-PA responses above levels achieved after administration of PA alone. We have previously reported that high levels of PA-specific Abs could be detected in mouse plasma following nasal immunization with PA doses of up to 25 μg when CT was used as adjuvant (35). The same studies showed that 40 μg of PA/dose were needed to promote PA-specific mucosal IgA Abs. The results summarized here indicated that ATR targeting with much lower doses of PA (i.e., 5 μg) and EF allows the induction of PA-specific S-IgA Abs. Interestingly, increasing the dose of PA given with EF to 40 μg did not increase the levels of PA-specific mucosal IgA Abs, suggesting that codelivery of EF achieved optimal S-IgA Ab responses with low nasal dose of PA. Although, nasal immunization with CT or LT-I as adjuvant primarily promotes IgA Ab responses in the respiratory and genitourinary tracts, low but significant responses are consistently seen in the gastrointestinal tract. PA was previously reported to deliver a functionally active CT-A subunit into mammalian cells using an LF^{1-254}-CT-A fusion protein (64). Therefore, it will be interesting to examine whether the ATR-mediated cellular targeting, the adenylate cyclase, and possibly other activities of EF govern the polarized PA-specific mucosal IgA Ab responses induced by EdTx as adjuvant.

In summary, we have shown that ATR targeting of an adenylate cyclase subunit provides an effective strategy for enhancing the immune response to nasal vaccines. The EdTx as nasal adjuvant does not target the olfactory or other CNS tissues and thus could represent a safer alternative to ganglioside-binding adjuvants. In addition, EdTx very efficiently promoted anti-PA Ab responses both in saliva and in plasma and this could have important implications for improving the efficacy of current PA-based anthrax vaccines.

Disclosures

The authors have no financial conflict of interest.

References

1. Mock, M., and A. Fouet. 2001. Anthrax. *Annu. Rev. Microbiol.* 55: 647–644.
2. Collier, R. J., and J. A. Young. 2003. Anthrax toxin. *Annu. Rev. Cell Dev. Biol.* 19: 45–70.
3. Moayeri, M., and S. H. Leppla. 2004. The roles of anthrax toxin in pathogenesis. *Curr. Opin. Microbiol.* 7: 19–24.
4. Bradley, K. A., J. Mogridge, M. Mourez, R. J. Collier, and J. A. Young. 2001. Identification of the cellular receptor for anthrax toxin. *Nature* 414: 225–229.
5. Scobie, H. M., G. J. Rainey, K. A. Bradley, and J. A. Young. 2003. Human capillary morphogenesis protein 2 functions as an anthrax toxin receptor. *Proc. Natl. Acad. Sci. USA* 100: 5170–5174.
6. Leppla, S. H. 1982. Anthrax toxin edema factor: a bacterial adenylate cyclase that increases cyclic AMP concentrations of eukaryotic cells. *Proc. Natl. Acad. Sci. USA* 79: 3162–3166.
7. Guo, Q., Y. Shen, N. L. Zhukovskaya, J. Florian, and W. J. Tang. 2004. Structural and kinetic analyses of the interaction of anthrax adenylyl cyclase toxin with reaction products cAMP and pyrophosphate. *J. Biol. Chem.* 279: 29427–29435.
8. Shen, Y., N. L. Zhukovskaya, Q. Guo, J. Florian, and W. J. Tang. 2005. Calcium-independent calmodulin binding and two-metal-ion catalytic mechanism of anthrax edema factor. *EMBO J.* 24: 929–941.
9. Singh, Y., S. H. Leppla, R. Bhatnagar, and A. M. Friedlander. 1989. Internalization and processing of *Bacillus anthracis* lethal toxin by toxin-sensitive and -resistant cells. *J. Biol. Chem.* 264: 11099–11102.
10. Friedlander, A. M., R. Bhatnagar, S. H. Leppla, L. Johnson, and Y. Singh. 1993. Characterization of macrophage sensitivity and resistance to anthrax lethal toxin. *Infect. Immun.* 61: 245–252.
11. Hanna, P. C., D. Acosta, and R. J. Collier. 1993. On the role of macrophages in anthrax. *Proc. Natl. Acad. Sci. USA* 90: 10198–10201.
12. Agrawal, A., J. Lingappa, S. H. Leppla, S. Agrawal, A. Jabbar, C. Quinn, and B. Pulendran. 2003. Impairment of dendritic cells and adaptive immunity by anthrax lethal toxin. *Nature* 424: 329–334.
13. Ballard, J. D., R. J. Collier, and M. N. Starnbach. 1996. Anthrax toxin-mediated delivery of a cytotoxic T-cell epitope in vivo. *Proc. Natl. Acad. Sci. USA* 93: 12531–12534.
14. Goletz, T. J., K. R. Klimpel, N. Arora, S. H. Leppla, J. M. Keith, and J. A. Berzofsky. 1997. Targeting HIV proteins to the major histocompatibility complex class I processing pathway with a novel gp120-anthrax toxin fusion protein. *Proc. Natl. Acad. Sci. USA* 94: 12059–12064.
15. Brossier, F., M. Weber-Levy, M. Mock, and J. C. Sirard. 2000. Protective antigen-mediated antibody response against a heterologous protein produced in vivo by *Bacillus anthracis*. *Infect. Immun.* 68: 5731–5734.
16. Lu, Y., R. Friedman, N. Kushner, A. Doling, L. Thomas, N. Touzjian, M. Starnbach, and J. Lieberman. 2000. Genetically modified anthrax lethal toxin safely delivers whole HIV protein antigens into the cytosol to induce T cell immunity. *Proc. Natl. Acad. Sci. USA* 97: 8027–8032.
17. Kushner, N., D. Zhang, N. Touzjian, M. Essex, J. Lieberman, and Y. Lu. 2003. A fragment of anthrax lethal factor delivers proteins to the cytosol without requiring protective antigen. *Proc. Natl. Acad. Sci. USA* 100: 6652–6657.
18. Price, B. M., A. L. Liner, S. Park, S. H. Leppla, A. Mateczun, and D. R. Galloway. 2001. Protection against anthrax lethal toxin challenge by genetic immunization with a plasmid encoding the lethal factor protein. *Infect. Immun.* 69: 4509–4515.
19. Kumar, P., N. Ahuja, and R. Bhatnagar. 2002. Anthrax edema toxin requires influx of calcium for inducing cyclic AMP toxicity in target cells. *Infect. Immun.* 70: 4997–5007.
20. Paccani, S. R., F. Tonello, R. Ghittoni, M. Natale, L. Muraro, M. M. D'Elios, W. J. Tang, C. Montecucco, and C. T. Baldari. 2005. Anthrax toxins suppress T lymphocyte activation by disrupting antigen receptor signaling. *J. Exp. Med.* 201: 325–331.
21. Spangler, B. D. 1992. Structure and function of cholera toxin and the related *Escherichia coli* heat-labile enterotoxin. *Microbiol. Rev.* 56: 622–647.
22. Gill, D. M. 1976. The arrangement of subunits in cholera toxin. *Biochemistry* 15: 1242–1248.
23. Gill, D. M., J. D. Clements, D. C. Robertson, and R. A. Finkelstein. 1981. Subunit number and arrangement in *Escherichia coli* heat-labile enterotoxin. *Infect. Immun.* 33: 677–682.
24. Heyningen, S. V. 1974. Cholera toxin: interaction of subunits with ganglioside GM1. *Science* 183: 656–657.
25. Holmgren, J., M. Lindblad, P. Fredman, L. Svennerholm, and H. Myrvold. 1985. Comparison of receptors for cholera and *Escherichia coli* enterotoxins in human intestine. *Gastroenterology* 89: 27–35.
26. Griffiths, S. L., R. A. Finkelstein, and D. R. Critchley. 1986. Characterization of the receptor for cholera toxin and *Escherichia coli* heat-labile toxin in rabbit intestinal brush borders. *Biochem. J.* 238: 313–322.
27. Fukuta, S., J. L. Magnani, E. M. Twiddy, R. K. Holmes, and V. Ginsburg. 1988. Comparison of the carbohydrate-binding specificities of cholera toxin and *Escherichia coli* heat-labile enterotoxins LTh-I, LT-IIa, and LT-IIb. *Infect. Immun.* 56: 1748–1753.
28. Couch, R. B. 2004. Nasal vaccination, *Escherichia coli* enterotoxin, and Bell's palsy. *N. Engl. J. Med.* 350: 860–861.
29. Mutsch, M., W. Zhou, P. Rhodes, M. Bopp, R. T. Chen, T. Linder, C. Spyr, and R. Steffen. 2004. Use of the inactivated intranasal influenza vaccine and the risk of Bell's palsy in Switzerland. *N. Engl. J. Med.* 350: 896–903.
30. van Ginkel, F. W., R. J. Jackson, Y. Yuki, and J. R. McGhee. 2000. Cutting edge: the mucosal adjuvant cholera toxin redirects vaccine proteins into olfactory tissues. *J. Immunol.* 165: 4778–4782.
31. Eriksson, A. M., K. M. Schon, and N. Y. Lycke. 2004. The cholera toxin-derived CTA1-DD vaccine adjuvant administered intranasally does not cause inflammation or accumulate in the nervous tissues. *J. Immunol.* 173: 3310–3319.
32. Ramirez, D. M., S. H. Leppla, R. Schneerson, and J. Shiloach. 2002. Production, recovery and immunogenicity of the protective antigen from a recombinant strain of *Bacillus anthracis*. *J. Ind. Microbiol. Biotechnol.* 28: 232–238.
33. Cooksey, B. A., G. C. Sampey, J. L. Pierre, X. Zhang, J. D. Karwoski, G. H. Choi, and M. W. Laird. 2004. Production of biologically active *Bacillus anthracis* edema factor in *Escherichia coli*. *Biotechnol. Prog.* 20: 1651–1659.
34. Boyaka, P. N., M. Ohmura, K. Fujihashi, T. Koga, M. Yamamoto, M. N. Kweon, Y. Takeda, R. J. Jackson, H. Kiyono, Y. Yuki, and J. R. McGhee. 2003. Chimeras of labile toxin one and cholera toxin retain mucosal adjuvanticity and direct Th cell subsets via their B subunit. *J. Immunol.* 170: 454–462.
35. Boyaka, P. N., A. Tafaro, R. Fischer, S. H. Leppla, K. Fujihashi, and J. R. McGhee. 2003. Effective mucosal immunity to anthrax: neutralizing antibodies and Th cell responses following nasal immunization with protective antigen. *J. Immunol.* 170: 5636–5643.
36. Mosmann, T. 1983. Rapid colorimetric assay for cellular growth and survival: application to proliferation and cytotoxicity assays. *J. Immunol. Methods* 65: 55–63.
37. Lillard, J. W., Jr., U. P. Singh, P. N. Boyaka, S. Singh, D. D. Taub, and J. R. McGhee. 2003. MIP-1α and MIP-1β differentially mediate mucosal and systemic adaptive immunity. *Blood* 101: 807–814.

38. Boyaka, P. N., M. Marinaro, R. J. Jackson, S. Menon, H. Kiyono, E. Jirillo, and J. R. McGhee. 1999. IL-12 is an effective adjuvant for induction of mucosal immunity. *J. Immunol.* 162: 122–128.
39. Livak, K. J., and T. D. Schmittgen. 2001. Analysis of relative gene expression data using real-time quantitative PCR and the $2(-\Delta\Delta C_T)$ method. *Methods* 25: 402–408.
40. Elson, C. O., and W. Ealding. 1984. Cholera toxin feeding did not induce oral tolerance in mice and abrogated oral tolerance to an unrelated protein antigen. *J. Immunol.* 133: 2892–2897.
41. Elson, C. O., and W. Ealding. 1984. Generalized systemic and mucosal immunity in mice after mucosal stimulation with cholera toxin. *J. Immunol.* 132: 2736–2741.
42. Clements, J. D., N. M. Hartzog, and F. L. Lyon. 1988. Adjuvant activity of *Escherichia coli* heat-labile enterotoxin and effect on the induction of oral tolerance in mice to unrelated protein antigens. *Vaccine* 6: 269–277.
43. Elson, C. O., and M. T. Dertzbaugh. 1999. Mucosal adjuvants. In *Mucosal Immunology*. P. L. Ogra, J. Mestecky, M. E. Lamm, W. Strober, J. Bienenstock, and J. R. McGhee, eds. Academic Press, San Diego, pp. 817–838.
44. Bromander, A. K., M. Kjerrulf, J. Holmgren, and N. Lycke. 1993. Cholera toxin enhances alloantigen presentation by cultured intestinal epithelial cells. *Scand. J. Immunol.* 37: 452–458.
45. Cong, Y., C. T. Weaver, and C. O. Elson. 1997. The mucosal adjuvanticity of cholera toxin involves enhancement of costimulatory activity by selective up-regulation of B7.2 expression. *J. Immunol.* 159: 5301–5308.
46. Yamamoto, M., H. Kiyono, M. N. Kweon, S. Yamamoto, K. Fujihashi, H. Kurazono, K. Imaoka, H. Bluethmann, I. Takahashi, Y. Takeda, et al. 2000. Enterotoxin adjuvants have direct effects on T cells and antigen-presenting cells that result in either interleukin-4-dependent or -independent immune responses. *J. Infect. Dis.* 182: 180–190.
47. Agren, L. C., L. Ekman, B. Lowenadler, and N. Y. Lycke. 1997. Genetically engineered nontoxic vaccine adjuvant that combines B cell targeting with immunomodulation by cholera toxin A1 subunit. *J. Immunol.* 158: 3936–3946.
48. Agren, L., E. Sverremark, L. Ekman, K. Schon, B. Lowenadler, C. Fernandez, and N. Lycke. 2000. The ADP-ribosylating CTA1-DD adjuvant enhances T cell-dependent and independent responses by direct action on B cells involving anti-apoptotic Bcl-2- and germinal center-promoting effects. *J. Immunol.* 164: 6276–6286.
49. Bonuccelli, G., F. Sotgia, P. G. Frank, T. M. Williams, C. J. de Almeida, H. B. Tanowitz, P. E. Scherer, K. A. Hotchkiss, B. I. Terman, B. Rollman, et al. 2005. Anthrax toxin receptor (ATR/TEM8) is highly expressed in epithelial cells lining the toxin's three sites of entry (lung, skin, and intestine). *Am. J. Physiol.* 288: C1402–C1410.
50. Beauregard, K. E., S. Wimer-Mackin, R. J. Collier, and W. I. Lencer. 1999. Anthrax toxin entry into polarized epithelial cells. *Infect. Immun.* 67: 3026–3030.
51. Doling, A. M., J. D. Ballard, H. Shen, K. M. Krishna, R. Ahmed, R. J. Collier, and M. N. Starnbach. 1999. Cytotoxic T-lymphocyte epitopes fused to anthrax toxin induce protective antiviral immunity. *Infect. Immun.* 67: 3290–3296.
52. Marinaro, M., H. F. Staats, T. Hiroi, R. J. Jackson, M. Coste, P. N. Boyaka, N. Okahashi, M. Yamamoto, H. Kiyono, H. Bluethmann, et al. 1995. Mucosal adjuvant effect of cholera toxin in mice results from induction of T helper 2 (Th2) cells and IL-4. *J. Immunol.* 155: 4621–4629.
53. Vajdy, M., M. H. Kosco-Vilbois, M. Kopf, G. Kohler, and N. Lycke. 1995. Impaired mucosal immune responses in interleukin 4-targeted mice. *J. Exp. Med.* 181: 41–53.
54. Takahashi, I., M. Marinaro, H. Kiyono, R. J. Jackson, I. Nakagawa, K. Fujihashi, S. Hamada, J. D. Clements, K. L. Bost, and J. R. McGhee. 1996. Mechanisms for mucosal immunogenicity and adjuvancy of *Escherichia coli* labile enterotoxin. *J. Infect. Dis.* 173: 627–635.
55. Okahashi, N., M. Yamamoto, J. L. Vancott, S. N. Chatfield, M. Roberts, H. Bluethmann, T. Hiroi, H. Kiyono, and J. R. McGhee. 1996. Oral immunization of interleukin-4 (IL-4) knockout mice with a recombinant *Salmonella* strain or cholera toxin reveals that $CD4^+$ Th2 cells producing IL-6 and IL-10 are associated with mucosal immunoglobulin A responses. *Infect. Immun.* 64: 1516–1525.
56. Kweon, M. N., M. Yamamoto, F. Watanabe, S. Tamura, F. W. Van Ginkel, A. Miyauchi, H. Takagi, Y. Takeda, T. Hamabata, K. Fujihashi, et al. 2002. A nontoxic chimeric enterotoxin adjuvant induces protective immunity in both mucosal and systemic compartments with reduced IgE antibodies. *J. Infect. Dis.* 186: 1261–1269.
57. Agren, L. C., L. Ekman, B. Lowenadler, J. G. Nedrud, and N. Y. Lycke. 1999. Adjuvanticity of the cholera toxin A1-based gene fusion protein, CTA1-DD, is critically dependent on the ADP-ribosyltransferase and Ig-binding activity. *J. Immunol.* 162: 2432–2440.
58. Lycke, N., A. K. Bromander, L. Ekman, U. Karlsson, and J. Holmgren. 1989. Cellular basis of immunomodulation by cholera toxin in vitro with possible association to the adjuvant function in vivo. *J. Immunol.* 142: 20–27.
59. Bromander, A., J. Holmgren, and N. Lycke. 1991. Cholera toxin stimulates IL-1 production and enhances antigen presentation by macrophages in vitro. *J. Immunol.* 146: 2908–2914.
60. McGee, D. W., C. O. Elson, and J. R. McGhee. 1993. Enhancing effect of cholera toxin on interleukin-6 secretion by IEC-6 intestinal epithelial cells: mode of action and augmenting effect of inflammatory cytokines. *Infect. Immun.* 61: 4637–4644.
61. Staats, H. F., and F. A. Ennis, Jr. 1999. IL-1 is an effective adjuvant for mucosal and systemic immune responses when coadministered with protein immunogens. *J. Immunol.* 162: 6141–6147.
62. Gagliardi, M. C., F. Sallusto, M. Marinaro, S. Vendetti, A. Riccomi, and M. T. De Magistris. 2002. Effects of the adjuvant cholera toxin on dendritic cells: stimulatory and inhibitory signals that result in the amplification of immune responses. *Int. J. Med. Microbiol.* 291: 571–575.
63. Yamamoto, S., H. Kiyono, M. Yamamoto, K. Imaoka, K. Fujihashi, F. W. Van Ginkel, M. Noda, Y. Takeda, and J. R. McGhee. 1997. A nontoxic mutant of cholera toxin elicits Th2-type responses for enhanced mucosal immunity. *Proc. Natl. Acad. Sci. USA* 94: 5267–5272.
64. Sharma, M., H. Khanna, N. Arora, and Y. Singh. 2000. Anthrax toxin-mediated delivery of cholera toxin-A subunit into the cytosol of mammalian cells. *Biotechnol. Appl. Biochem.* 32(Pt. 1): 69–72.

CCR7 Is Critically Important for Migration of Dendritic Cells in Intestinal Lamina Propria to Mesenteric Lymph Nodes[1]

Myoung Ho Jang,[2]* Nagako Sougawa,[2]* Toshiyuki Tanaka,* Takako Hirata,† Takachika Hiroi,‡ Kazuo Tohya,§ Zijin Guo,* Eiji Umemoto,* Yukihiko Ebisuno,* Bo-Gie Yang,* Ju-Young Seoh,¶ Martin Lipp,‖ Hiroshi Kiyono,‡ and Masayuki Miyasaka[3]*

Although dendritic cells (DCs) located in the small intestinal lamina propria (LP-DCs) migrate to mesenteric lymph nodes (MLNs) constitutively, it is unclear which chemokines regulate their trafficking to MLNs. In this study we report that LP-DCs in unperturbed mice require CCR7 to migrate to MLNs. In vitro, LP-DCs expressing CCR7 migrated toward CCL21, although the LP-DCs appeared morphologically and phenotypically immature. In MLNs, DCs bearing the unique LP-DC phenotype ($CD11c^{high}CD8\alpha^{int}CD11b^{low}\alpha_L{}^{low}\beta_7{}^{high}$ and $CD11c^{high}CD8\alpha^{-}CD11b^{high}\alpha_L{}^{low}\beta_7{}^{high}$) were abundant in wild-type mice, but were markedly fewer in CCL19-, CCL21-Ser-deficient *plt/plt* mice and were almost absent in CCR7-deficient mice, indicating the critical importance of CCR7 in LP-DC trafficking to MLNs. Interestingly, $CCR7^{+}$ DCs in MLNs with the unique LP-DC phenotype had numerous vacuoles containing cellular debris in the cytoplasm, although MLN-DCs themselves were poorly phagocytic, suggesting that the debris was derived from the LP, where the LP-DCs ingested apoptotic intestinal epithelial cells (IECs). Consistent with this, LP-DCs ingested IECs vigorously in vitro. By presenting IEC-associated Ag, the LP-DCs also induce T cells to produce IL-4 and IL-10. Collectively, these results strongly suggest that LP-DCs with unique immunomodulatory activities migrate to MLNs in a CCR7-dependent manner to engage in the presentation of IEC-associated Ags acquired in the LP. *The Journal of Immunology,* **2006, 176: 803–810.**

Dendritic cells (DCs)[4] are cardinal constituents of the immune system and play pivotal roles in the induction of Ag-specific immune responses and the maintenance of self-tolerance (1). DCs are abundant in the small intestine, both in organized lymphoid tissues (Peyer's patches (PPs) and isolated lymphoid follicles (ILFs)) and in the lamina propria (LP), the layer of connective tissue between the epithelium and the muscularis mucosa, where they act as sentinels for incoming Ags. The precise discrimination between harmless Ags and dangerous pathogens by these DCs is a likely key mechanism for the maintenance of gut immune homeostasis (2).

Among the intestinal DCs, the DC subsets in PPs have been characterized in the most detail (3–6). PP-DCs can educate Ag-specific T cells to produce IL-4 and IL-10 (3) and confer gut-homing specificity on T cells (7, 8), indicating that they have unique immune-inductive abilities. In contrast, LP-DCs have been only incompletely characterized, mainly due to difficulty in isolating them. Recent investigations have revealed, however, that LP-DCs of a certain subset extend dendrites in a CX_3CR1-dependent manner to the luminal side of the gut for the uptake of Ags (9, 10). In addition, LP-DCs that reside in the terminal ileum sample commensal bacteria and constitutively express IL-12 p40, indicating that these LP-DCs may be involved in the predisposition to chronic inflammation (11). LP-DCs may also be important in the presentation of bacterial Ags directly to LP B cells (12, 13). LP-DCs obtained from mice treated with Flt3 (FMS-like tyrosine kinase 3) ligand, express high levels of IL-10 and type I IFN and can induce a state of immune hyporesponsiveness upon in vivo transfer (14), suggesting that LP-DCs may have an immunomodulatory role in the gut.

Apart from the LP-DCs, a distinct DC subset has been documented in rat intestinal lymph that can constitutively endocytose apoptotic intestinal epithelial cells (IECs) and transport them to the T cell areas of mesenteric lymph nodes (MLNs). However, it remains unclear whether these DCs are derived from the LP, PPs, and/or other intestinal compartment(s). In addition, their function remains unexplored, although they have been implicated in tolerance induction (15). It has been separately reported that among DCs in the MLNs, the $CD8\alpha^{-}CD11b^{+}$ DC subset plays a critical role in inducing cross-tolerance to food Ags, although it remains to be determined whether these DCs take up dying IECs (16).

DCs are thought to leave peripheral tissues when they receive an inflammatory or danger signal. During this process, DCs begin to mature, and the expression of CCR7 increases (17–19), which allows the DCs to enter lymph vessels and gain access to T cell areas

*Laboratory of Immunodynamics, Department of Microbiology and Immunology, Osaka University Graduate School of Medicine, and †21st Century Center of Excellence Program, Research Institute for Microbial Diseases, Osaka University, Osaka, Japan; ‡Division of Mucosal Immunology, Institute of Medical Science, University of Tokyo, Tokyo, Japan; §Department of Anatomy, Kansai College of Oriental Medicine, Osaka, Japan; ¶Department of Microbiology, College of Medicine, Ewha Woman's University, Seoul, Korea; and ‖Max Delbrück Center for Molecular Medicine, Berlin, Germany

Received for publication September 12, 2005. Accepted for publication October 28, 2005.

The costs of publication of this article were defrayed in part by the payment of page charges. This article must therefore be hereby marked *advertisement* in accordance with 18 U.S.C. Section 1734 solely to indicate this fact.

[1] This work was supported by a Grant-in-Aid from the Ministry of Education, Culture, Sports, Science, and Technology of Japan, and a grant for Advanced Research on Cancer from the Ministry of Education, Culture, Sports, Science, and Technology of Japan.

[2] M.H.J. and N.S. contributed equally to this work.

[3] Address correspondence and reprint requests to Dr. Masayuki Miyasaka, Laboratory of Immunodynamics, Department of Microbiology and Immunology, Osaka University Graduate School of Medicine, C8, 2-2 Yamada-oka, Suita 565-0871, Japan. E-mail address: mmiyasak@orgctl.med.osaka-u.ac.jp

[4] Abbreviations used in this paper: DC, dendritic cell; IEC, intestinal epithelial cell; ILF, isolated lymphoid follicle; LN, lymph node; LP, lamina propria; MLN, mesenteric lymph node; PP, Peyer's patch; SP-DC, splenic DC.

Copyright © 2006 by The American Association of Immunologists, Inc.

0022-1767/06/$02.00

in draining lymph nodes (LNs) in a CCR7-dependent manner (20). Corroborating this, a deficiency of CCR7 or its ligands, CCL19 and CCL21, leads to impaired DC migration into draining LNs and abnormal lymph node architecture in peripheral tissues (21, 22). In addition, a recent study indicates that steady-state trafficking of skin DCs to the draining LNs in peripheral tissues is also regulated by CCR7-mediated signaling (23). However, it is not known whether this commonly held paradigm of DC trafficking being driven by CCR7-mediated signaling holds true for DCs in the intestinal compartment as well.

In the present study we found that there are at least two LP-DC subsets in the intestinal LP of unperturbed mice and that they both require CCR7 for their constitutive migration to the MLNs. They vigorously ingest apoptotic IECs and, hence, are likely to correspond to the cells identified by Huang et al. (15) in rat mesenteric lymph. As suggested previously (15), LP-DCs can present IEC-associated Ags to $CD4^+$ T cells, inducing their differentiation into IL-4- and IL-10-producing cells. These results strongly indicate that LP-DCs bearing a unique immunomodulatory activity migrate constitutively to MLNs in a CCR7-dependent manner, thus generating a noninflammatory environment in the MLNs.

Materials and Methods

Mice

BALB/c mice were obtained from CLEA Japan. C57BL/6 mice were obtained from Japan SLC. Mice transgenic for a TCR that recognizes the $OVA_{323-339}$ peptide in the context of $I\text{-}A^d$ (DO 11.10 TCR-$\alpha\beta$ transgenic mice) on the BALB/c background were a gift from Dr. S. Ono (Osaka University Graduate School of Medicine, Osaka, Japan). The *plt/plt* mice on the B6 background were provided by Dr. H. Nakano (Duke University Medical Center, Raleigh, NC). CCR7-deficient mice on the C57BL/6 background were produced as previously described (21). All animal experiments were performed under an experimental protocol approved by the ethics review committee for animal experimentation of Osaka University Graduate School of Medicine.

Preparation of DCs from small intestinal LP, PPs, MLNs, and spleen

Small intestinal segments and PPs were treated with PBS containing 10% FCS, 20 mM HEPES, 100 U/ml penicillin, 100 μg/ml streptomycin, 1 mM sodium pyruvate, 10 mM EDTA, and 10 μg/ml polymyxin B (Calbiochem) for 30 min at 37°C to remove epithelial cells and were washed extensively with PBS. Small intestinal segments, PPs, MLNs, and spleen were digested with 400 Mandl units/ml collagenase D (Roche) and 10 μg/ml DNase I (Roche) in RPMI 1640/10% FCS with continuous stirring at 37°C for 45–90 min. EDTA was added (10 mM final concentration), and the cell suspension was incubated for an additional 5 min at 37°C. Cells were spun through a 15.5% Accudenz (Accurate Chemical & Scientific) solution to enrich for DCs. The obtained cells were incubated with FITC-conjugated anti-CD11b and PE-conjugated anti-CD11c after FcR blocking. DC subsets were sorted on the basis of their expression of CD11c and CD11b by FACSVantage SE (BD Biosciences). The purity of the sorted DCs was routinely >95%. For the morphological study, cytospin preparations from purified DC subsets were stained with May-Grunwald-Giemsa solution.

Double immunofluorescence staining of small intestinal LP

To determine the location of LP-DCs in the small intestinal LP, biotinylated anti-CD11c and FITC-conjugated anti-CD11b mAbs were applied overnight at 4°C to sections cut from frozen tissue. Samples were washed and then incubated with streptavidin-Alexa 594 (Molecular Probes) for 2 h at room temperature. To detect $CCR7^+$ DCs in the small intestinal LP, frozen sections of the small intestine were stained with rabbit anti-mouse CCR7 pAb, provided by Dr. K. Matsushima (University of Tokyo School of Medicine, Tokyo, Japan) and biotinylated anti-CD11c mAb overnight at 4°C. The sections were washed and then further incubated with Alexa 488-conjugated chicken anti-rabbit IgG Ab (Molecular Probes) and streptavidin-Alexa 594 for 2 h at room temperature. Immunohistochemical staining was analyzed with a Radiance 2100/Bio-Rad confocal laser microscope (Bio-Rad).

Flow cytometry

Fluorochrome-conjugated anti-CD11c (HL3), anti-CD11b (M1/70), and anti-CD8α (53-6.7) mAbs were used for DC staining. Anti-mouse CD16/CD32 (2.4G2) was used for FcR blocking. The expression of integrins was determined using mAbs to integrin α_L (CD11a; M17/4) and β_7 (M293). The expression of costimulatory molecules was determined using mAbs to B7-1 (CD80; 16-10A1), B7-2 (CD86; GL1), CD40 (3/23), and $I\text{-}A^d$ (AMS-32.1). These reagents were all purchased from BD Pharmingen. After the FcRs were blocked for 15 min at 4°C, the cells were stained for integrins, CD8α, CD11c, CD11b, and costimulatory molecules and then analyzed with a FACSCalibur (BD Biosciences). The DCs were identified by gating on the $CD11c^{high}$ cells. CCR7 expression by DCs was determined using the CCL19-Fc chimeric protein provided by Drs. K. Hieshima and O. Yoshie (Kinki University School of Medicine, Kinki, Japan).

RT-PCR for chemokine receptor expression

Total RNA was prepared from freshly isolated LP-DC using TRIzol (Invitrogen Life Technologies). RT of total RNA was conducted using oligo$(dT)_{18}$ primer and SensiScript reverse transcriptase (Qiagen). PCR was conducted using primer pairs for CCR1 (sense, AGAAGCCTACCCCA CAAC; antisense, TGGCCAGGTATCTGTCAA), CCR7 (sense, GGTGT GCCTCTGCCAAGA; antisense, TGCCAAAGATGCCCTTAC), CCR9 (sense, TGCTACTGGAGACAACTTCG; antisense, CTCCTCAGAACT GCAGTTAC), and β-actin (sense, ATGGATGACGATATCGCT; antisense, ATGAGGTAGTCTGTCAGGT) and Ex-*Taq* polymerase (Takara Shuzo). The PCR conditions were 30 cycles at 97, 57, and 72°C for 30 s each, and the products were analyzed on agarose gels.

Chemotaxis assays

All cell suspensions and chemokine dilutions were made in RPMI 1640 containing 0.5% low endotoxin BSA (Sigma-Aldrich). The chemokine CCL21 was purchased from Techne. Chemotactic assays were performed as previously described (24). Two hours after the start of migration, the inserts were removed. Migrated DCs were identified on a FACSCalibur using FITC-conjugated anti-CD11b mAb and PE-conjugated anti-CD11c mAb.

Real-time chemotaxis assay

Real-time chemotaxis assays were performed as previously described (25). To count the migrated cells in each channel, images of the cells in each channel were digitally recorded onto a computer hard disk with time-lapse intervals of 60 s.

Detection of apoptotic IECs in MLN-DCs

To detect IECs-derived apoptotic DNA in DCs, cytospin preparations from FACS-sorted MLN-DCs were fixed with 1% paraformaldehyde and stained using an ApopTag peroxidase in situ apoptosis detection kit (Serologicals) Detection of alkaline phosphatase activity in the FACS-sorted $CD11c^{high}CD8\alpha^{int}\alpha_L{}^{low}\beta_7{}^{high}$ MLN-DC subset was performed using the Vector Red Alkaline Phosphatase Substrate Kit I (Vector Laboratories).

Electron microscopy

Isolated cells were spun at 400 × *g* and fixed in 1% in glutaraldehyde in 0.1 M phosphate buffer for 1 h at 4°C. After being washed, the cells were embedded in 2% agarose gel and postfixed in 2% osmium tetroxide in 0.1 M phosphate buffer for 2 h at 4°C. The fixed samples were then dehydrated in a graded ethanol series, infiltrated with propylene oxide, and embedded in Quetol 812 epoxy resin. Ultrathin sections were stained with 2% uranyl acetate and Reynold's lead citrate, then examined using a JEOL JEM-1230 electron microscope.

In vitro uptake of CFSE-labeled apoptotic epithelial cells by DCs

Small IECs were obtained as described previously (26). IECs were then labeled with CFSE (Molecular Probes) at a concentration of 5 μM for 5 min at 37°C and cultured for 4 h to induce spontaneous apoptosis. Enriched DCs were mixed with CFSE-labeled apoptotic IECs and cultured for 4 h at 37°C. After the coculture, cells were stained with PE-conjugated anti-CD11c mAb and allophycocyanin-conjugated anti-CD11b mAb to identify the DC subsets. The uptake of apoptotic IECs by DCs was evaluated by FACSCalibur.

Analysis of $CD4^+$ T cell proliferation and cytokine production

IECs obtained as described above were loaded with OVA (Sigma-Aldrich) by osmotic shock (27). They were then cocultured with DCs for 4 h, and

the DC subsets were subsequently sorted on the basis of their expression of CD11c and CD11b. Purified DCs (5×10^3) and DO11.10 OVA TCR-transgenic T cells (1×10^5) were mixed in 96-well plates (1/20). After 7 days, the cells were collected and stained with anti-mouse DO11.10 TCR (KJ1-26; Caltag Laboratories) and anti-mouse CD4 (RM4-5) mAbs. Dead cells were excluded using 7-aminoactinomycin D (Sigma-Aldrich). T cell proliferation was measured by CFSE dilution. To examine cytokine secretion, DO11.10 $CD4^+$ T cells were cocultured with IEC-OVA-containing DCs for 14 days (two-round stimulation with IEC-OVA-containing DCs with a 7-day interval). The T cells were then washed and restimulated for 6 h with anti-CD3 mAb in the presence of monensin (BD Pharmingen). Intracellular cytokine staining was performed according to the manufacturer's instructions (BD Pharmingen).

Results

Small intestinal LP contains two distinct DC subsets

We first determined the localization of LP-DC subsets in the small intestine by immunohistochemistry. As shown in Fig. 1*A*, cells that were $CD11b^-/CD11c^+$ (open arrowheads) and $CD11b^+/CD11c^+$ (filled arrowheads) were readily recognizable in the LP, indicating that the small intestinal LP contains at least two phenotypically distinguishable DC subsets.

We next attempted to isolate LP-DCs and successfully obtained substantial numbers of low density leukocytes from the LP ($1.95 \pm 0.5 \times 10^6$ cells/mouse; $n = 34$), of which the $CD11c^+$ DCs constituted ~10–15%. Among these cells, at least two LP-DC subsets could be recognized on the basis of their different CD11c/CD11b expression patterns: $CD11c^{high}CD11b^{low}$ (R1; 4.9 ± 2.0% of low density cells) and $CD11c^{high}CD11b^{high}$ (R2; 8.4 ± 2.0%; Fig. 1*B*). The remaining cells, which were $CD11c^{int}CD11b^{high}$, consisted mainly of cells that contained eosinophilic granules (J.-H. Seoh and M. H. Jang, manuscript in preparation). The $CD11c^{high}$ LP-DC subsets were heterogeneous in their CD8α expression, in that the $CD11c^{high}CD11b^{low}$ subset expressed CD8α at an intermediate level ($CD8\alpha^{int}$), whereas the $CD11c^{high}CD11b^{high}$ subset was $CD8\alpha^-$ (Fig. 1*B*). Thus, the phenotypes of the R1 and R2 subsets were $CD11c^{high}CD8\alpha^{int}CD11b^{low}$ and $CD11c^{high}CD8\alpha^-CD11b^{high}$, respectively.

These two subsets were found not only in the intestines of $Id2^{-/-}$ mice, which are completely deficient in PPs and ILFs (28), but also in the BALB/c small intestine from which PPs and ILFs had been surgically removed before the isolation procedure (data not shown), suggesting that they are indeed derived from the small intestinal LP and not PPs or ILFs. Interestingly, the freshly isolated R1 and R2 subsets both had few dendrites. The nuclear chromatin was not very condensed, and the cytoplasm was light blue to grayish when stained with May-Grunwald-Giemsa solution, suggesting that the LP-DCs were not fully mature (Fig. 1*C*).

The expression of costimulatory molecules also supported the idea that these cells were somewhat immature. As shown in Fig. 1*D*, LP-DCs showed substantially lower expression of MHC class II and CD40 than DCs from PPs and MLNs, indicating that they were less mature than other DCs in the intestinal compartment. Interestingly, however, the LP-DCs displayed a relatively high expression level of B7-2, as seen in PP-DCs, if not as high as that expressed by MLN-DCs, indicating that the LP-DCs may not be entirely immature but, rather, may constitute semimature subsets. The $CD11c^{high}$ LP-DC subsets were DEC-205^+, but $B220^-$ and Gr-1^- (data not shown), indicating that they are distinct from plasmacytoid DCs (29) or the recently identified $CD70^+$ APCs (30) in the LP, both of which express readily detectable levels of DEC-205, B220, and Gr-1.

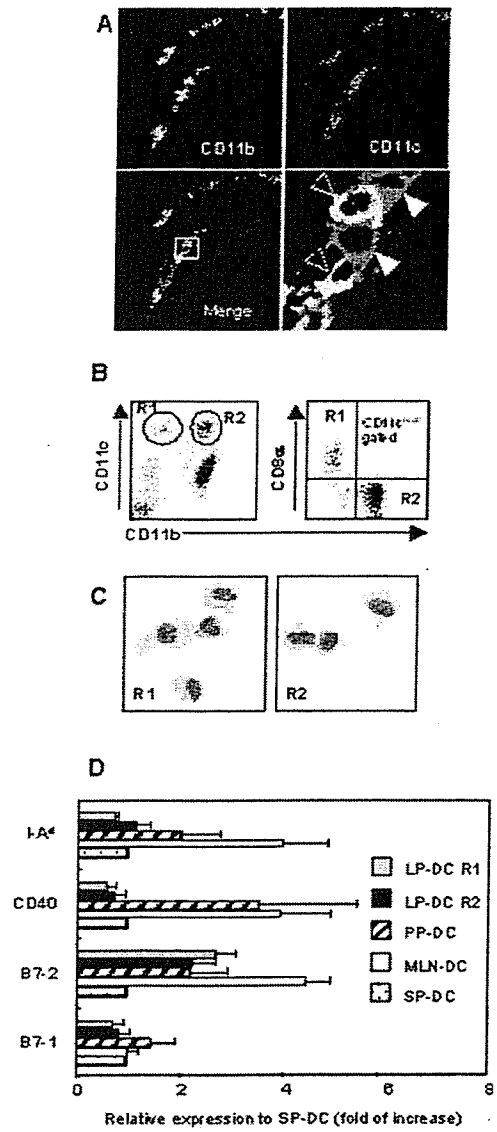

FIGURE 1. Identification of two DC subpopulations in the LP of the small intestine. *A*, Frozen sections of small intestine were fixed, stained with Abs specific for CD11b (green) and CD11c (red), and analyzed by confocal microscopy. Two cell subsets, $CD11b^-CD11c^+$ (red; open arrowheads) and $CD11b^+CD11c^+$ (yellow; filled arrowheads) were readily identifiable within the LP. *B*, Low density lamina propria cells were isolated from the small intestines of BALB/c mice and spun through a 15.5% Accudenz gradient. Enriched DCs were stained for CD8α, CD11b, and CD11c and analyzed by flow cytometry. *C*, Two DC subsets (R1 ($CD11c^{high}CD8\alpha^{int}CD11b^{low}$) and R2 ($CD11c^{high}CD8\alpha^-CD11b^{high}$)) were FACS-sorted based on their CD11c and CD11b expressions and stained with May-Grunwald-Giemsa. The R1 and R2 subsets had a morphology associated with highly motile cells. *D*, The LP-DC subsets had a semimature phenotype. DC subsets from LP, PPs, MLNs, and spleen (SP) were stained for CD11c, CD11b, and B7-1, B7-2, CD40, or $I\text{-}A^d$ and analyzed by flow cytometry. The expression levels are shown as the ratio of the mean fluorescence intensity (MFI) to the fluorescence intensity of SP-DCs.

LP-DC subsets express CCR7 and show directional migration toward CCL21

Although steady-state trafficking of DCs from the skin to the draining LNs is regulated by CCR7-mediated signaling (23), it remains to be established whether LP-DC trafficking is also regulated by a

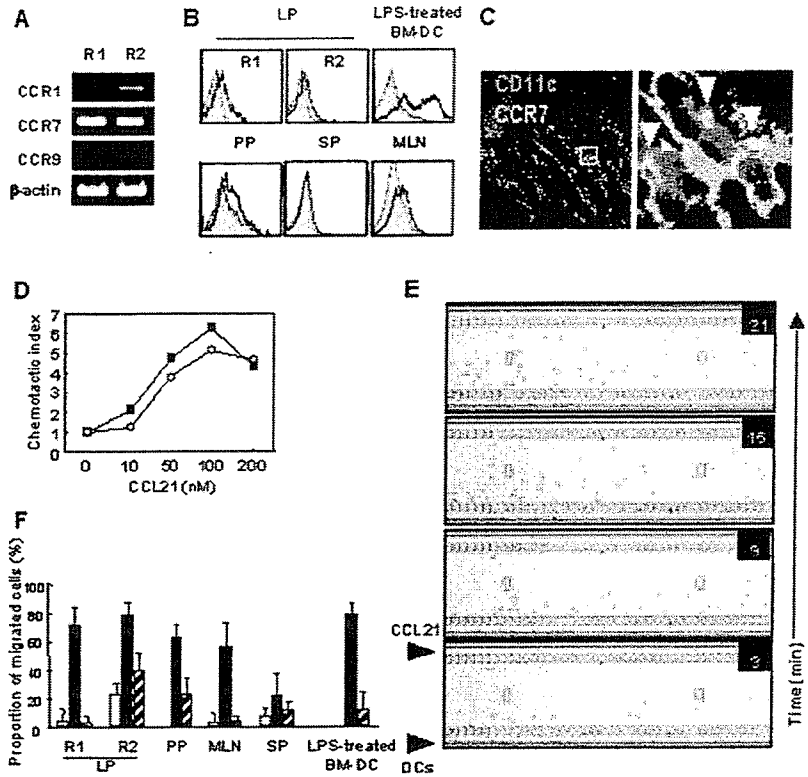

FIGURE 2. LP-DC subsets express CCR7 and show directional migration toward CCL21. *A*, Expression of CCR7 mRNA. cDNA was prepared from total RNA obtained from freshly FACS-sorted LP-DCs, and the expression of chemokine receptors was analyzed by semiquantitative PCR. *B*, Expression of CCR7 protein on the cell surface. DCs were stained for CCR7 using the CCL19-Fc chimera protein (□). LPS-stimulated bone marrow-derived DC was used as a positive control, and human Ig Fc protein served as a negative control (▨). *C*, Localization of $CCR7^+/CD11c^+$ DCs in the small intestinal LP. Frozen sections of the small intestine were fixed and stained with anti-CCR7 pAb and biotinylated anti-CD11c mAb. The sections were further incubated with Alexa 488-conjugated secondary Ab and streptavidin-Alexa 594. Arrows indicate $CCR7^+/CD11c^+$ cells. *D*, Chemotaxis analysis by Transwell. LP-DCs were placed in the upper well of a Transwell apparatus (5-μm pore size), and an increasing concentration of CCL21 was added to the lower well for 2 h. The migrated cells were stained for CD11c and CD11b, then analyzed by FACSCalibur. The proportion of migrated cells in each population was calculated as a fraction of the input population. The chemotactic index is shown as the ratio of the proportion of cells that migrated in the presence of chemokine to the proportion that migrated in the absence of chemokine. ■, R1 subset; ○, R2 subset. *E*, Time-lapse video monitoring of chemotaxis. Isolated LP-DCs were applied to the microchemotaxis chamber. After aligning the cells on the edge of the microchannel of the chamber, CCL21 (10 μM) was applied to the opposite side of the microchannel (see *top* of each frame), so that a concentration gradient of the chemokine formed from the top to the bottom of the channel. The migration of cells in the microchannel was subsequently monitored at 6-min intervals. Note that a significant fraction of the cells had begun migrating from the bottom to the top of the field 15–21 min after the addition of CCL21. *F*, Quantitative evaluation of chemotactic responses to CCL21. Data are shown as the proportion of cells that migrated across the microchannel to the total cells in the assay area. □, Medium alone; ■, CCL21; ▨, CCL21 with PTX treatment. The data are representative of at least three independent experiments.

CCR7-dependent mechanism. We thus examined CCR7 expression in LP-DCs. In the R1 ($CD11c^{high}CD11b^{low}$) and R2 ($CD11c^{high}CD11b^{high}$) subsets, CCR7 mRNA was highly expressed, whereas CCR9 mRNA was absent (Fig. 2*A*). Consistent with this, LP-DCs were $CCR7^+$, as evidenced by their binding of a CCL19-fusion protein (Fig. 2*B*), and $CD11c^+$ DCs expressing CCR7 were readily detectable in the LP by immunohistochemistry (Fig. 2*C*). Furthermore, in vitro, the $CD11c^{high}$ LP-DCs efficiently migrated through Transwell inserts in response to CCL21 with the typical bell-shaped dose-response curve that is characteristic of chemotaxis (Fig. 2*D*). To verify that this reflects directional, but not random, migration, we adopted an optical chemotaxis assay system that allows time-lapse video monitoring of cell behavior in silicon-coated microchannels (25). As shown in Fig. 2*E* and supplemental movie A,[5] LP-DCs moved swiftly along the CCL21 concentration gradient, verifying that they can migrate directionally toward a CCL21 source as a result of expressing functional CCR7. Compared with DCs from other tissues, LP-DCs showed much stronger chemotaxis toward CCL21 than splenic DCs (SP-DCs), but their chemotaxis was comparable to that seen in MLN-DCs and PP-DCs (Fig. 2*F*). LPS-stimulated, bone marrow-derived DCs responded to CCL21 much like the LP-DC subsets. In all these cell types, CCL21-mediated migration was significantly blocked by pertussis toxin. These data indicate that LP-DCs with relatively immature morphology and phenotype can migrate toward CCL21 as efficiently as mature DCs without deliberate inflammatory stimulation.

LP-DCs migrate to MLNs in a CCR7-dependent manner

We next investigated whether LP-DCs could be identified in the MLNs and, if so, whether their migration was dependent on CCR7. Because a recent study indicated that DC migrants to lymph nodes could be discriminated by their surface phenotype (31), we first compared the expressions of various surface markers on the $CD11c^{high}$ DCs obtained from the LP, PPs, MLNs, and spleen. As shown in Fig. 3*A*, LP-DCs highly expressed β_7 integrin compared with other DCs. In this regard, LP-DCs contained $CD8\alpha^{int}\beta_7{}^{high}$ and $CD8\alpha^-\beta_7{}^{high}$ subpopulations, which correspond to the R1 and

[5] The online version of this article contains supplemental material.

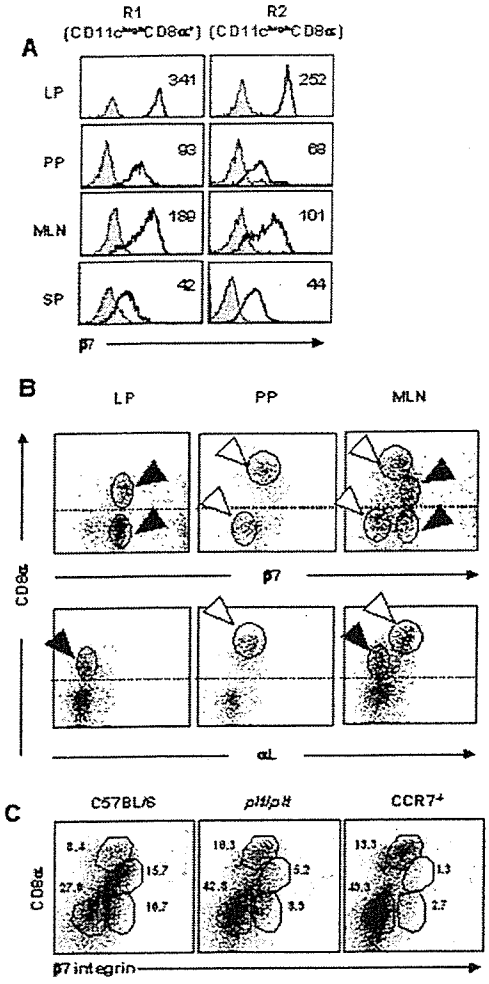

FIGURE 3. Apparent CCR7 dependency of the CD8$\alpha^{int}\beta_7^{high}$ and CD8$\alpha^-\beta_7^{high}$ subsets in MLNs. *A*, LP-DCs highly expressed β_7 integrin compared with other DCs. Low density cells from the LP were stained for CD11c, CD8α, and β_7 integrin, and the histogram profiles were acquired after gating on CD11c^{high}CD8α^+ DCs (R1) or CD11c^{high}CD8α^- DCs (R2). ▨, Isotype controls; □, stained cells. The numbers in the histograms indicate the MFI. *B*, LP-DCs and PP-DCs appear to constitute the MLN-DCs. Low density cells from the LP were double stained for CD8α/integrin β_7 or for CD8α/integrin α_L. FACS profiles were acquired after gating on the CD11c^{high} cells. Based on the CD8α/integrin β_7 double staining, the MLN-DCs consisted of four recognizable subsets, with two of them phenotypically corresponding to LP-DCs (filled arrowheads) and the remaining two corresponding to PP-DCs (open arrowheads). A similar observation was made with CD8α/integrin α_L double staining; MLN-DCs showed two CD8α^+ subsets, one of which corresponded phenotypically to an LP-DC subset (filled arrowhead) and the other to a PP-DC subset (open arrowhead). *C*, CD8$\alpha^{int}\beta_7^{high}$ and CD8$\alpha^-\beta_7^{high}$ LP-DCs were significantly fewer in the MLNs of *plt/plt* mice and were almost absent from the MLNs of CCR7-deficient mice. Numbers indicate the percentage of each subset within gated CD11c^{high} cells.

R2 subsets, respectively, and the PP-DCs had CD8$\alpha^{high}\beta_7^{int}$ and CD8$\alpha^-\beta_7^{low}$ populations. In contrast, the MLN-DCs contained all four surface phenotypes, supporting the possibility that LP-DCs and PP-DCs enter the MLNs to make up the four different DC subsets there (Fig. 3*B*). Furthermore, the examination of α_L expression in CD8α^+ DCs revealed that those in the LP expressed relatively low levels of α_L (CD8$\alpha^{int}\alpha_L^{low}$), whereas those in PPs expressed high levels of α_L (CD8$\alpha^{high}\alpha_L^{high}$), and the MLN-DCs consisted of both populations (Fig. 3*B*). These observations thus suggest that the MLNs collect phenotypically different DCs from the LP and PPs, in accordance with the MLNs being the draining LNs of the LP and PPs.

We next asked whether these intestinal DCs enter the draining MLNs in a manner dependent on CCR7. For this purpose, we examined MLN-DCs in wild-type C57BL/6 mice; in C57BL/6-*plt/plt* mice, which are deficient in CCL19/CCL21-Ser (22); and in CCR7-deficient mice (21) that had been backcrossed to the C57BL/6 genetic background. As shown in Fig. 3*C*, the CD8$\alpha^{int}\beta_7^{high}$ and CD8$\alpha^-\beta_7^{high}$ subsets (R1 and R2 in the LP, respectively) represented subsets of the MLN-DCs of wild-type mice (15.7 and 10.7% of the total CD11c^{high} DCs, respectively), but these subsets were significantly less prominent (5.2 and 8.9%) in the MLNs of *plt/plt* mice, which lack CCL21-Ser, but express CCL21-Leu, in their lymphatics, and were almost totally absent (1.3 and 2.7%) in the MLNs of CCR7-deficient mice. These results strongly suggest that both the R1 and R2 LP-DC subsets migrate to the MLNs in a CCR7-dependent manner under steady-state conditions. Consistent with this, both these LP-DC subsets were present in the intestine of CCR7-deficient mice (M. H. Jang and N. Sougawa, unpublished observation).

We also found that the majority of MLN-DCs were CCR7$^+$, as evidenced by their binding of a CCL19 fusion protein (Fig. 2*B*), and like the unique DCs documented in rat intestinal lymph by Huang et al. (15), MLN-DCs contained much debris in the cytoplasm (Fig. 4*A*). The pieces of debris were TUNEL positive, that is, they showed apoptosis-induced DNA fragmentation (Fig. 4*B*). In addition, a considerable proportion of these cells contained granules that were positive for alkaline phosphatase (Fig. 4*C*), which is expressed in epithelial cells, but not DCs. In contrast, the MLN-DCs themselves showed little phagocytic activity, as described below. These results are compatible with the idea that the CCR7$^+$ MLN-DCs were derived from the LP in a CCR7-dependent manner, after having ingested apoptotic IECs in the LP.

LP-DCs efficiently endocytose apoptotic epithelial cells

Because IECs undergo apoptosis extensively in situ, and because the DCs containing apoptotic epithelial cells are found in mesenteric lymph (15), we examined whether LP-DCs are unique in their ability to take up apoptotic IECs by observing isolated LP-DCs by transmission electron microscopy. As shown in Fig. 4*D*, the cytoplasm of the R1 cells contained numerous inclusions of 1–1.5 μm in diameter with membranous materials inside them, suggesting that these cells have a high phagocytic activity for apoptotic cells. The cytoplasm of the R2 subset contained fewer, but nonetheless distinct, phagocytic vesicles, a conspicuous Golgi network, well-developed rough endoplasmic reticulum, and numerous round mitochondria, suggesting that R2 is less phagocytic, but more active in protein synthesis and secretion, than R1. Both subsets showed a few finger-like protrusions from the cell body, with the protrusions from R2 cells being finer than those from R1 cells. These observations indicate that LP-DCs are highly active in the metabolism and phagocytosis of apoptotic cells.

Consistent with the above findings, in vitro analysis showed that both LP-DC subsets were highly phagocytic, efficiently and vigorously taking up CFSE-labeled apoptotic IECs (Fig. 4*E*), with the R1 subset taking up these cells more avidly than the R2 subset, as evidenced by conspicuous IEC-associated fluorescence staining in the cytoplasm (Fig. 4*F*). PP-DCs were heterogeneous in their phagocytic activity, with the CD11b$^-$ fraction of the population taking up apoptotic cells efficiently, and the CD11b$^+$ population showing less activity. In contrast, the MLN-DCs had little phagocytic activity regardless of their CD11b expression, and CD11b$^-$ SP-DCs showed intermediate levels of phagocytosis.

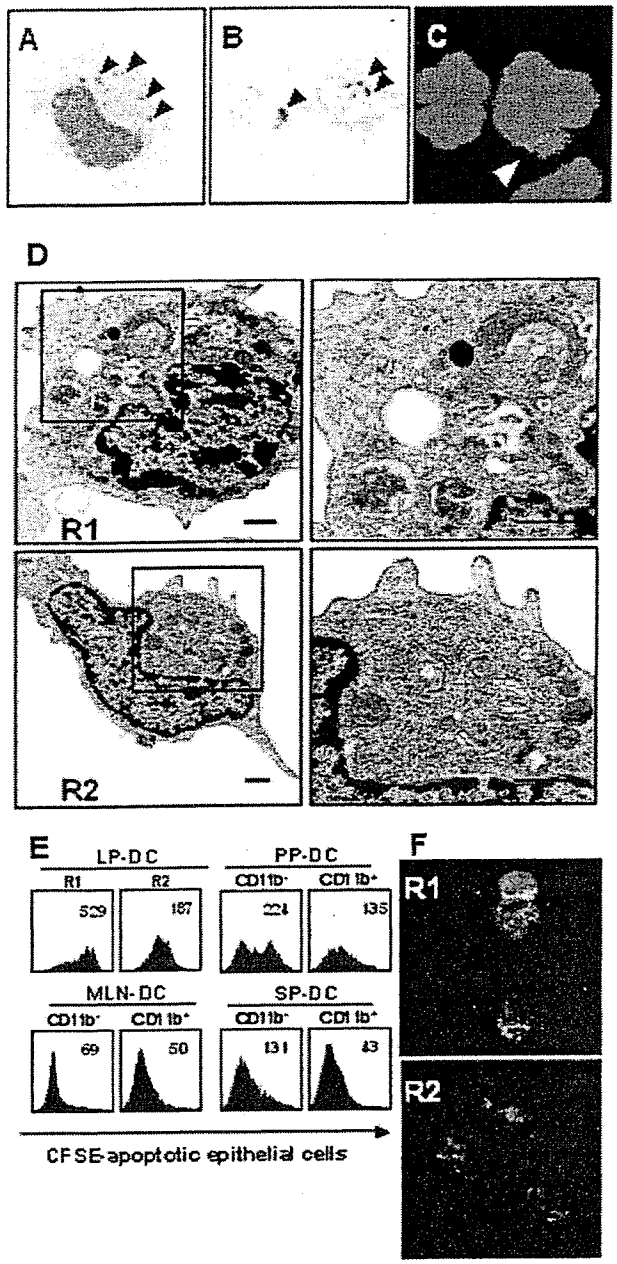

FIGURE 4. LP-DC subsets efficiently endocytose apoptotic IECs. *A–C*, The cytoplasm of MLN-DCs bearing the unique LP-DC phenotype contains cellular debris and fragmented DNA. *A*, FACS-sorted $CD11c^{high}CD8\alpha^{int}\alpha_L{}^{low}\beta_7{}^{high}$ MLN-DC stained with May-Grunwald-Giemsa shows abundant cellular debris in the cytoplasm. *B*, Two $CD11c^{high}CD8\alpha^{int}\alpha_L{}^{low}\beta_7{}^{high}$ MLN-DCs show TUNEL-positive inclusions. *C*, A $CD11c^{high}CD8\alpha^{int}\alpha_L{}^{low}\beta_7{}^{high}$ MLN-DC shows alkaline phosphatase-positive inclusions in the cytoplasm. *D*, Representative transmission electron microscopic views of cells from the LP-DC R1 (*upper*) and R2 (*lower*) subsets. All bars = 1 μm. *E*, Enriched DCs were cocultured with CFSE-labeled apoptotic IECs for 4 h. The DCs were then collected and stained for CD11c and CD11b and analyzed by flow cytometry. The numbers in the histograms indicate the MFI. *F*, Confocal microscopic images showing the uptake of CFSE-labeled apoptotic IECs by LP-DCs.

LP-DCs presenting IEC-associated Ag induce the differentiation of IL-10- and IL-4-producing $CD4^+$ T cells

We next investigated whether LP-DCs could present Ag associated with apoptotic cells to T cells. For this purpose, freshly isolated IECs from the small intestine were intracellularly loaded with OVA by osmotic shock and then allowed to undergo apoptosis spontaneously. Subsequently, the OVA-loaded apoptotic IECs were cocultured with DCs for 4 h, and the Ag-pulsed DC subsets were subjected to cell sorting. The purified DCs were then cocultured with DO11.10 T cells for 6 days, and T cell proliferation was measured by CFSE dilution. As shown in Fig. 5*A*, both the LP-DC subsets induced vigorous T cell proliferation, whereas a subset of SP-DCs, $CD11b^-$ SP-DCs, which displayed moderate phagocytic activity, induced slightly less T cell proliferation than the LP-DCs. The $CD11b^+$ SP-DCs, which had much less phagocytic activity than the LP-DCs, induced only weak proliferation. These results show that LP-DCs can take up apoptotic cells and present cell-associated Ags to T cells more potently than splenic DCs.

Mucosal DCs from the PPs and lungs tend to induce Th2 responses in T cell priming assays (3, 32). We therefore addressed whether LP-DCs also show this tendency by examining the cytokine secretion of OVA TCR-transgenic $CD4^+$ T cells primed by LP-DCs that had been exposed to OVA-loaded apoptotic IECs. As shown in Fig. 5*B*, T cells primed by LP-DCs expressed significantly higher levels of IL-4 and IL-10 than did SP-DC-primed T

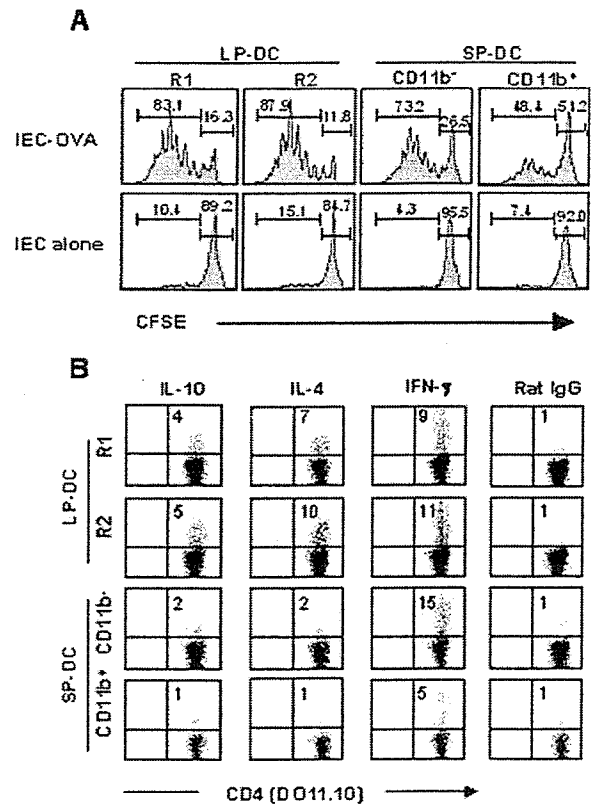

FIGURE 5. LP-DC subsets present IEC-associated Ags. *A*, LP-DC subsets induced cell-associated, Ag-specific T cell proliferation. Freshly isolated IECs were intracellularly loaded with OVA by osmotic shock, then allowed to undergo apoptosis spontaneously. LP-DCs were cocultured with the apoptotic IECs for 4 h, and the DCs were sorted using a FACSVantage SE. Subsequently, purified DCs bearing the OVA-containing IECs were cultured with naive DO11.10 T cells for 6 days. *B*, The LP-DCs primed DO11.10 T cells to produce IL-4 and IL-10. DCs bearing OVA-containing IECs were then cultured with DO11.10 T cells for 14 days (two rounds of stimulation with a 7-day interval). For intracellular cytokine staining, the T cells were restimulated with the anti-CD3ε mAb for 6 h in the presence of monensin. The data are representative of three independent experiments. Numbers within a quadrant indicate the percentage of cytokine-producing cells.

cells. The production of IFN-γ was comparable among the T cells primed with the different DCs. These results indicate that LP-DCs have a propensity to induce IL-4- and IL-10-producing T cells when exposed to Ag associated with apoptotic IECs.

Discussion

In this study we showed that there are at least two LP-DC subsets in the intestinal LP of unperturbed mice, and they both require CCR7 for their constitutive migration to MLNs. As speculated previously (15), LP-DCs can, in fact, present Ag associated with apoptotic IECs to naive $CD4^+$ T cells to induce the differentiation of IL-4- and IL-10-producing T cells. These observations indicate that LP-DCs with unique immunomodulatory activities migrate to MLNs in a CCR7-dependent manner to engage in the presentation of IEC-associated Ags from apoptotic IECs that were phagocytosed locally; this may help explain how a noninflammatory immune response can be maintained in MLNs under steady-state conditions.

Although it is generally accepted that DC migration is largely under the control of chemokines and chemokine receptors, studies of the molecules responsible for the migration of LP-DCs to MLNs in the steady state are lacking. The almost complete absence of DCs bearing the LP-DC phenotype ($CD11c^{high}CD8\alpha^{int}\beta_7^{high}$ and $CD11c^{high}CD8\alpha^-\beta_7^{high}$) in the MLNs of CCR7-deficient mice and their marked reduction in the MLNs of *plt/plt* mice, as shown in this study, provide strong evidence that CCR7 is critically important for LP-DC migration to the MLNs. Our unpublished observation that LP-DCs were found in the intestines of CCR7-deficient mice also supports this hypothesis. The ligands for CCR7 are CCL19 and CCL21. The *plt/plt* mouse strain congenitally lacks the expression of CCL19 and CCL21-Ser, but does express another CCL21 gene product, CCL21-Leu, in lymphatic endothelial cells (20). Thus, our data point to a critical role for CCR7-mediated signaling at the step of DC entry into the intestinal lymphatics, although additional investigation is required to pinpoint the site(s) of action of CCR7-mediated signaling. A pivotal role for CCR7 in the migration of skin DCs to afferent dermal lymphatics has been indicated in a report by Ohl et al. (23).

CCR7-mediated signaling may also play a role in the maturation and survival of LP-DCs transported to the MLNs, because CCR7 has been shown to induce antiapoptotic signaling (33) and terminal activation (34) in DCs. Although this issue could, in theory, be investigated by comparing the fate of CCR7-deficient vs wild-type LP-DCs within MLNs upon their injection into the intestinal lymphatics, a technical difficulty involved in applying this procedure to the mouse has prevented us from performing such experiments.

It is of note that although LP-DCs appeared to be relatively immature, showing a $CD80^{low}CD86^{int}$MHC class $II^{low}CD40^{low}$ phenotype, they expressed CCR7 and functionally responded avidly to CCL21 like mature DCs (19, 35). Given that immature DCs, albeit CCR7 negative initially, up-regulate their CCR7 expression upon ingestion of opsonized apoptotic cells (36), it is tempting to speculate that LP-DCs acquire CCR7 expression through the ingestion of apoptotic IECs in situ.

In contrast to the LP-derived DCs, the number of PP-derived DCs ($CD8\alpha^{high}\beta_7^{int}$ and $CD8\alpha^-\beta_7^{low}$) was not lower in the MLNs of *plt/plt* and CCR7-deficient mice (Fig. 4), indicating that PP-DCs do not depend on CCR7 signaling for migration to the MLNs. Previous studies showed that different PP-DC subsets differentially express multiple chemokine receptors, including CCR1, CCR2, CCR5, CCR7, CCR9, and CCR10, with all the subsets expressing functional CCR7 (4, 37). Although PP-DCs may use CCR7-mediated signaling for their localization within PP microdomains, as suggested previously (4), our study indicates that PP-DCs depend on non-CCR7 ligand chemokine(s) for their steady-state migration to MLNs.

Although recent studies of murine LP-DCs have identified several distinct subsets, i.e., $CD11c^+CD8\alpha^-CD11b^+$ (14, 38), $CD11c^+CD8\alpha^-CD11b^-$ (11, 14), $CD11c^+CD8\alpha^+CD11b^-$, $CD11c^{int}CD8\alpha^-CD11b^+B220^+$ (14), and $CD11c^-CD11b^-$ (30), our data presented in this paper clearly showed that, among these groups, the major contributors are from two populations, i.e., $CD11c^{high}CD8\alpha^{int}CD11b^{low}\alpha_L^{low}\beta_7^{high}$ (R1) and $CD11c^{high}CD8\alpha^-CD11b^{high}\alpha_L^{low}\beta_7^{high}$ (R2), in unperturbed mice. We also observed $CD11c^{int}CD11b^{high}$ cells to be abundant in the LP, but we did not include them in our current analysis, because they appeared to be different from conventional DCs, with numerous cytoplasmic eosinophilic granules. There were also low numbers of DC-like cells in our LP cell population, but they constituted only a very small proportion of the cells compared with R1 and R2, and thus they were not analyzed in the current study.

The recently reported $CD11c^+CD8\alpha^-CD11b^-$ LP-DCs constitutively expressing the IL-12 p40 promoter (11) and APCs with the $CD11c^-CD11b^-$ phenotype that constitutively express CD70 (30) may have been among the cell populations we did not study. In addition, a recent study identified $CX3CR1^+$ LP-DCs that form dendrites through the IECs of the terminal ileum to sample bacteria in the lumen directly (10). Because these $CX3CR1^+$ LP-DCs are $CD11c^{high}CD11b^{high}$, they resemble the R2 subset of our analysis. However, our preliminary observation indicates that hardly any cells in the R2 subset were reactive with an anti-CX_3CR1 mAb (M. H. Jang and N. Sougawa, unpublished observation).

Previous reports by Huang et al. (15) using mesenteric lymphadenectomized rats showed a DC subset in the intestinal lymph that constitutively transports apoptotic IECs to the T cell areas in MLNs. Our study demonstrated that although MLN-DCs with the LP-DC phenotype are poorly phagocytic, there is irrefutable evidence of previous phagocytosis, inasmuch as they contain much intracytoplasmic cellular debris, and both $CD8\alpha^{int}$ and $CD8\alpha^-$ LP-DC subsets can ingest apoptotic IECs vigorously and present IEC-associated Ag to $CD4^+$ T cells in vitro. These results strongly indicate that MLN-DCs containing considerable cellular debris correspond to the cells identified in the intestinal lymph by Huang et al. (15), and that the site of apoptotic cell acquisition by these cells is the LP.

Our observation that LP-DCs could polarize $CD4^+$ T cell differentiation to favor IL-4- and IL-10-producing T cells subsequent to coculture with Ag-loaded apoptotic IECs parallels the observation by Iwasaki and Kelsall (3) that PP-DCs generate T cells that produce high levels of IL-4 and IL-10 and less IFN-γ, as well as the observation by Alpan et al. (39) that Ag-loaded DCs present in MLNs can induce T cells to produce IL-4 and IL-10. Thus, certain intestinal DCs, including the LP-DCs, may have a tendency to induce Th2, rather than Th1, cells, which may be, at least in part, related to their localization to a specific microenvironment. Because phagocytosis of apoptotic cells has been reported to result in an anti-inflammatory state via transcriptional suppression of IL-12 (40), DCs that are closely colocalized with IECs in the LP may become locally imprinted not to induce Th1 cells upon ingestion of apoptotic IECs. In addition, conditioned medium of IECs have been shown to induce DCs to release IL-6 and to prime Th2 responses (41). Thus, the local microenvironment appears to confer on DCs a propensity to induce Th2 cells.

Collectively, these data provide strong evidence that CCR7 is critical for the recruitment of LP-DCs into the MLNs under steady-state conditions. Because these LP-DCs phagocytose apoptotic IECs and present IEC-associated Ag to induce IL-4- and IL-10-producing $CD4^+$ T cells, they are likely to be involved in the

immunomodulation of T cells within the MLNs. Thus, our study strengthens the idea that CCR7 is involved in the maintenance of peripheral tolerance (23) and points to a role for CCR7 in the recruitment of immunomodulatory DCs to the MLNs.

Acknowledgments

We thank Drs. S. Ono, H. Nakano, Y. Takahama, K. Matsushima, K. Hieshima, and O. Yoshie for providing valuable reagents and/or animals, and Dr. H. Hayasaka for critical reading of the manuscript. We also thank S. Yamashita and M. Komine for secretarial assistance, and Y. Nakano for technical help.

Disclosures

The authors have no financial conflict of interest.

References

1. Banchereau, J., F. Briere, C. Caux, J. Davoust, S. Lebecque, Y. J. Liu, B. Pulendran, and K. Palucka. 2000. Immunobiology of dendritic cells. *Annu. Rev. Immunol.* 18: 767–811.
2. Kelsall, B. L., and M. Rescigno. 2004. Mucosal dendritic cells in immunity and inflammation. *Nat. Immunol.* 5: 1091–1095.
3. Iwasaki, A., and B. L. Kelsall. 1999. Freshly isolated Peyer's patch, but not spleen, dendritic cells produce interleukin 10 and induce the differentiation of T helper type 2 cells. *J. Exp. Med.* 190: 229–239.
4. Iwasaki, A., and B. L. Kelsall. 2000. Localization of distinct Peyer's patch dendritic cell subsets and their recruitment by chemokines macrophage inflammatory protein (MIP)-3α, MIP-3β, and secondary lymphoid organ chemokine. *J. Exp. Med.* 191: 1381–1394.
5. Iwasaki, A., and B. L. Kelsall. 2001. Unique functions of CD11b$^+$, CD8α^+, and double-negative Peyer's patch dendritic cells. *J. Immunol.* 166: 4884–4890.
6. Kelsall, B. L., and W. Strober. 1996. Distinct populations of dendritic cells are present in the subepithelial dome and T cell regions of the murine Peyer's patch. *J. Exp. Med.* 183: 237–247.
7. Mora, J. R., M. R. Bono, N. Manjunath, W. Weninger, L. L. Cavanagh, M. Rosemblatt, and U. H. Von Andrian. 2003. Selective imprinting of gut-homing T cells by Peyer's patch dendritic cells. *Nature* 424: 88–93.
8. Iwata, M., A. Hirakiyama, Y. Eshima, H. Kagechika, C. Kato, and S. Y. Song. 2004. Retinoic acid imprints gut-homing specificity on T cells. *Immunity* 21: 527–538.
9. Rescigno, M., M. Urbano, B. Valzasina, M. Francolini, G. Rotta, R. Bonasio, F. Granucci, J. P. Kraehenbuhl, and P. Ricciardi-Castagnoli. 2001. Dendritic cells express tight junction proteins and penetrate gut epithelial monolayers to sample bacteria. *Nat. Immunol.* 2: 361–367.
10. Niess, J. H., S. Brand, X. Gu, L. Landsman, S. Jung, B. A. McCormick, J. M. Vyas, M. Boes, H. L. Ploegh, J. G. Fox, et al. 2005. CX_3CR1-mediated dendritic cell access to the intestinal lumen and bacterial clearance. *Science* 307: 254–258.
11. Becker, C., S. Wirtz, M. Blessing, J. Pirhonen, D. Strand, O. Bechthold, J. Frick, P. R. Galle, I. Autenrieth, and M. F. Neurath. 2003. Constitutive p40 promoter activation and IL-23 production in the terminal ileum mediated by dendritic cells. *J. Clin. Invest.* 112: 693–706.
12. Fagarasan, S., and T. Honjo. 2004. Regulation of IgA synthesis at mucosal surfaces. *Curr. Opin. Immunol.* 16: 277–283.
13. Fagarasan, S., K. Kinoshita, M. Muramatsu, K. Ikuta, and T. Honjo. 2001. In situ class switching and differentiation to IgA-producing cells in the gut lamina propria. *Nature* 413: 639–643.
14. Chirdo, F. G., O. R. Millington, H. Beacock-Sharp, and A. M. Mowat. 2005. Immunomodulatory dendritic cells in intestinal lamina propria. *Eur. J. Immunol.* 35: 1831–1840.
15. Huang, F. P., N. Platt, M. Wykes, J. R. Major, T. J. Powell, C. D. Jenkins, and G. G. MacPherson. 2000. A discrete subpopulation of dendritic cells transports apoptotic intestinal epithelial cells to T cell areas of mesenteric lymph nodes. *J. Exp. Med.* 191: 435–444.
16. Chung, Y., J. H. Chang, M. N. Kweon, P. D. Rennert, and C. Y. Kang. 2005. CD8α^-11b$^+$ dendritic cells but not CD8α^+ dendritic cells mediate cross-tolerance toward intestinal antigens. *Blood* 106: 201–206.
17. Chan, V. W., S. Kothakota, M. C. Rohan, L. Panganiban-Lustan, J. P. Gardner, M. S. Wachowicz, J. A. Winter, and L. T. Williams. 1999. Secondary lymphoid-tissue chemokine (SLC) is chemotactic for mature dendritic cells. *Blood* 93: 3610–3616.
18. Dieu, M. C., B. Vanbervliet, A. Vicari, J. M. Bridon, E. Oldham, S. Ait-Yahia, F. Briere, A. Zlotnik, S. Lebecque, and C. Caux. 1998. Selective recruitment of immature and mature dendritic cells by distinct chemokines expressed in different anatomic sites. *J. Exp. Med.* 188: 373–386.
19. Sallusto, F., P. Schaerli, P. Loetscher, C. Schaniel, D. Lenig, C. R. Mackay, S. Qin, and A. Lanzavecchia. 1998. Rapid and coordinated switch in chemokine receptor expression during dendritic cell maturation. *Eur. J. Immunol.* 28: 2760–2769.
20. von Andrian, U. H., and T. R. Mempel. 2003. Homing and cellular traffic in lymph nodes. *Nat. Rev. Immunol.* 3: 867–878.
21. Forster, R., A. Schubel, D. Breitfeld, E. Kremmer, I. Renner-Muller, E. Wolf, and M. Lipp. 1999. CCR7 coordinates the primary immune response by establishing functional microenvironments in secondary lymphoid organs. *Cell* 99: 23–33.
22. Gunn, M. D., S. Kyuwa, C. Tam, T. Kakiuchi, A. Matsuzawa, L. T. Williams, and H. Nakano. 1999. Mice lacking expression of secondary lymphoid organ chemokine have defects in lymphocyte homing and dendritic cell localization. *J. Exp. Med.* 189: 451–460.
23. Ohl, L., M. Mohaupt, N. Czeloth, G. Hintzen, Z. Kiafard, J. Zwirner, T. Blankenstein, G. Henning, and R. Forster. 2004. CCR7 governs skin dendritic cell migration under inflammatory and steady-state conditions. *Immunity* 21: 279–288.
24. Kellermann, S. A., S. Hudak, E. R. Oldham, Y. J. Liu, and L. M. McEvoy. 1999. The CC chemokine receptor-7 ligands 6Ckine and macrophage inflammatory protein-3β are potent chemoattractants for in vitro- and in vivo-derived dendritic cells. *J. Immunol.* 162: 3859–3864.
25. Kanegasaki, S., Y. Nomura, N. Nitta, S. Akiyama, T. Tamatani, Y. Goshoh, T. Yoshida, T. Sato, and Y. Kikuchi. 2003. A novel optical assay system for the quantitative measurement of chemotaxis. *J. Immunol. Methods* 282: 1–11.
26. Yamamoto, M., K. Fujihashi, K. Kawabata, J. R. McGhee, and H. Kiyono. 1998. A mucosal intranet: intestinal epithelial cells down-regulate intraepithelial, but not peripheral, T lymphocytes. *J. Immunol.* 160: 2188–2196.
27. Haan, J. d., S. Lehar, and M. Bevan. 2000. CD8$^+$ but not CD8$^-$ dendritic cells cross-prime cytotoxic T cells in vivo. *J. Exp. Med.* 192: 1685–1696.
28. Yokota, Y., A. Mansouri, S. Mori, S. Sugawara, S. Adachi, S. Nishikawa, and P. Gruss. 1999. Development of peripheral lymphoid organs and natural killer cells depends on the helix-loop-helix inhibitor Id2. *Nature* 397: 702–706.
29. Nakano, H., M. Yanagita, and M. D. Gunn. 2001. CD11c$^+$B220$^+$Gr-1$^+$ cells in mouse lymph nodes and spleen display characteristics of plasmacytoid dendritic cells. *J. Exp. Med.* 194: 1171–1178.
30. Laouar, A., V. Haridas, D. Vargas, X. Zhinan, D. Chaplin, R. A. van Lier, and N. Manjunath. 2005. CD70$^+$ antigen-presenting cells control the proliferation and differentiation of T cells in the intestinal mucosa. *Nat. Immunol.* 6: 698–706.
31. Ardavin, C. 2003. Origin, precursors and differentiation of mouse dendritic cells. *Nat. Rev. Immunol.* 3: 582–590.
32. Akbari, O., R. H. DeKruyff, and D. T. Umetsu. 2001. Pulmonary dendritic cells producing IL-10 mediate tolerance induced by respiratory exposure to antigen. *Nat. Immunol.* 2: 725–731.
33. Sanchez-Sanchez, N., L. Riol-Blanco, G. de la Rosa, A. Puig-Kroger, J. Garcia-Bordas, D. Martin, N. Longo, A. Cuadrado, C. Cabanas, A. L. Corbi, et al. 2004. Chemokine receptor CCR7 induces intracellular signaling that inhibits apoptosis of mature dendritic cells. *Blood* 104: 619–625.
34. Marsland, B. J., P. Battig, M. Bauer, C. Ruedl, U. Lassing, R. R. Beerli, K. Dietmeier, L. Ivanova, T. Pfister, L. Vogt, et al. 2005. CCL19 and CCL21 induce a potent proinflammatory differentiation program in licensed dendritic cells. *Immunity* 22: 493–505.
35. Yanagihara, S., E. Komura, J. Nagafune, H. Watarai, and Y. Yamaguchi. 1998. EBI1/CCR7 is a new member of dendritic cell chemokine receptor that is up-regulated upon maturation. *J. Immunol.* 161: 3096–3102.
36. Verbovetski, I., H. Bychkov, U. Trahtemberg, I. Shapira, M. Hareuveni, O. Ben-Tal, I. Kutikov, O. Gill, and D. Mevorach. 2002. Opsonization of apoptotic cells by autologous iC3b facilitates clearance by immature dendritic cells, down-regulates DR and CD86, and up-regulates CC chemokine receptor 7. *J. Exp. Med.* 196: 1553–1561.
37. Zhao, X., A. Sato, C. S. Dela Cruz, M. Linehan, A. Luegering, T. Kucharzik, A. K. Shirakawa, G. Marquez, J. M. Farber, I. Williams, et al. 2003. CCL9 is secreted by the follicle-associated epithelium and recruits dome region Peyer's patch CD11b$^+$ dendritic cells. *J. Immunol.* 171: 2797–2803.
38. Anjuere, F., C. Luci, M. Lebens, D. Rousseau, C. Hervouet, G. Milon, J. Holmgren, C. Ardavin, and C. Czerkinsky. 2004. In vivo adjuvant-induced mobilization and maturation of gut dendritic cells after oral administration of cholera toxin. *J. Immunol.* 173: 5103–5111.
39. Alpan, O., G. Rudomen, and P. Matzinger. 2001. The role of dendritic cells, B cells, and M cells in gut-oriented immune responses. *J. Immunol.* 166: 4843–4852.
40. Kim, S., K. B. Elkon, and X. Ma. 2004. Transcriptional suppression of interleukin-12 gene expression following phagocytosis of apoptotic cells. *Immunity* 21: 643–653.
41. Rimoldi, M., M. Chieppa, V. Salucci, F. Avogadri, A. Sonzogni, G. M. Sampietro, A. Nespoli, G. Viale, P. Allavena, and M. Rescigno. 2005. Intestinal immune homeostasis is regulated by the crosstalk between epithelial cells and dendritic cells. *Nat. Immunol.* 6: 507–514.

Cutting Edge: Uniqueness of Lymphoid Chemokine Requirement for the Initiation and Maturation of Nasopharynx-Associated Lymphoid Tissue Organogenesis[1]

Satoshi Fukuyama, Takahiro Nagatake,* Dong-Young Kim,* Kaoru Takamura,* Eun Jeong Park,* Tsuneyasu Kaisho,† Norimitsu Tanaka,‡ Yuichi Kurono,‡ and Hiroshi Kiyono[2]**

CD3$^-$CD4$^+$CD45$^+$ inducer cells are required for the initiation of mucosa-associated organogenesis of both nasopharynx-associated lymphoid tissues (NALT) and Peyer's patches (PP) in the aerodigestive tract. CXCL13$^{-/-}$ mice and mice carrying the paucity of lymph node T cell (plt) mutation and lacking expression of CCL19 and CCL21 accumulate CD3$^-$CD4$^+$CD45$^+$ cells at the site of NALT but not of PP genesis. Although NALT was observed to develop in adult CXCL13$^{-/-}$ and plt/plt mice, the formation of germinal centers in CXCL13$^{-/-}$ mice was affected, and their population of B cells was much lower than in the NALT of CXCL13$^{+/-}$ mice. Similarly, fewer T cells were observed in the NALT of plt/plt mice than in control mice. These findings indicate that the initiation of NALT organogenesis is independent of CXCL13, CCL19, and CCL21. However, the expression of these lymphoid chemokines is essential for the maturation of NALT microarchitecture. The Journal of Immunology, 2006, 177: 4276–4280.

Nasopharynx-associated lymphoid tissue (NALT)[3] plays a pivotal role in the initiation of Ag-specific immune responses at both systemic and mucosal sites (1). Thus, NALT acts as an important inductive site for the generation of Ag-specific IgA-committed B cells (1). In addition, although NALT possesses a predominance of naive Th0 CD4$^+$ cells, the Ag-specific Th1 and/or Th2 immune responses can be induced in NALT through intranasal administration of Ags and mucosal adjuvants (e.g., cholera toxin) (1). Thus, NALT is thought to be a key secondary lymphoid structure for the upper respiratory tract.

The lymphotoxin (LT)βR signaling pathway is essential for the organogenesis of secondary lymphoid tissues, including peripheral lymph nodes (LN) and Peyer's patches (PP) (2). However, previous reports by our and other groups (3, 4) have demonstrated that NALT organogenesis, unlike that of other secondary lymphoid tissues, can occur independently of the LTβR signaling pathway. Inducer cells with phenotypes of CD3$^-$, CD4$^+$, and CD45$^+$ are required for the initiation of the organogenesis of NALT, PP, and LN (1–3). Lymphoid chemokines, including CXCL13, CCL19, and CCL21, have been shown to be important for the recruitment of CD3$^-$CD4$^+$CD45$^+$ cells to the PP anlagen (5, 6). Not surprisingly then, CXCR5$^{-/-}$ mice and CXCL13$^{-/-}$ mice lack PP and several types of LN such as inguinal and iliac LN (7). Although PP and LN are developed in mice carrying the paucity of LN T cell (*plt*) mutation, which are known not to produce CCR7 ligands, CCL19 and CCL21, a study using double mutants of CXCL13$^{-/-}$ and *plt/plt* mice revealed that CCL19, CCL21, and CXCL13 were cooperatively involved in the development of secondary lymphoid organs (7). However, little is known about the involvement of these lymphoid chemokines for the recruitment of CD3$^-$CD4$^+$CD45$^+$ cells to sites of NALT development.

To better understand the varying roles of lymphoid chemokines in the development of NALT and the maintenance of its architecture, we investigated the unique characteristics of NALT development using CXCL13$^{-/-}$ mice and *plt/plt* mice. Our results provide the first evidence that the initiation of NALT organogenesis is independent of lymphoid chemokines,

*Division of Mucosal Immunology, Department of Microbiology and Immunology, The Institute of Medical Science, The University of Tokyo, Tokyo, Japan; †RIKEN Research Center for Allergy and Immunology, Yokohama, Japan; and ‡Department of Otolaryngology, Head and Neck Surgery, Kagoshima University Graduate School of Medical and Dental Sciences, Kagoshima, Japan

Received for publication May 8, 2006. Accepted for publication August 1, 2006.

The costs of publication of this article were defrayed in part by the payment of page charges. This article must therefore be hereby marked *advertisement* in accordance with 18 U.S.C. Section 1734 solely to indicate this fact.

[1] This work was supported by the Core Research for Evolutional Science and Technology Program, from Japan Science and Technology Corporation, and a Grant-in-Aid from the Ministry of Education, Science, Sports, and Culture and the Ministry of Health and Welfare of Japan. S.F. was supported by research fellowships from the Japan Society for the Promotion of Science for Young Scientists. D.-Y.K. was supported by research fellowships from the Japan Society for the Promotion of Science for Foreign Researchers.

[2] Address correspondence and reprint requests to Dr. Hiroshi Kiyono, Division of Mucosal Immunology, Department of Microbiology and Immunology, The Institute of Medical Science, The University of Tokyo, 4-6-1 Shirokanedai, Minato-ku, Tokyo 108-8639, Japan. E-mail address: kiyono@ims.u-tokyo.ac.jp

[3] Abbreviations used in this paper: NALT, nasopharynx-associated lymphoid tissue; PP, Peyer's patch; LT, lymphotoxin; LN, lymph node; E17, 17-day-old embryo; LDM, laser microdissection; FDC, follicular dendritic cell; PNA, peanut agglutinin; NALTi, NALT inducer cell; PPi, PP inducer cell; MLN, mesenteric LN.

Copyright © 2006 by The American Association of Immunologists, Inc.

0022-1767/06/$02.00

including CXCL13, CCL19, and CCL21. Lymphoid chemokines have been shown to play an important role in the maturation of the microarchitecture of secondary lymphoid organs (8, 9), and our current findings show that these same chemokines are essential for NALT microarchitecture formation as well.

Materials and Methods

Mice

BALB/c and C57BL/6 mice were purchased from Japan SLC. The procedure for generating CXCL13$^{-/-}$ mice on a C57BL/6 background was reported previously (10). *Plt/plt* mice with a BALB/c background were provided from Drs. H. Nakano and T. Kakiuchi (Department of Immunology, Toho University School of Medicine, Tokyo, Japan) (11). CXCL13$^{-/-}$*plt/plt* mice were generated by intercrossing CXCL13$^{-/-}$ mice with *plt/plt* mice. PCR primers D4Mit237 (sense, 5′-TTCAAACTCATGAGTCTATGGGG-3′; antisense, 5′-ATATACACGTAGACTCGCACGC-3′) were used to determine the genome type of *plt/plt* and *plt/+* or +/+ (11).

Cell analysis and isolation by flow cytometry

Cells were isolated from the nasal tissues and intestines and then stained with the appropriate fluorescence-conjugated anti-CD3ε (145-2C11; BD Pharmingen), anti-CD45 (30-F11; BD Pharmingen), anti-CD4 (L3T4; BD Pharmingen), anti-B220 (RA3-6B2; BD Pharmingen), anti-CD11c (HL3; BD Pharmingen), anti-CXCR5 (2G8; BD Pharmingen), and/or anti-CCR7 (4B12; eBioscience) (3). Cells were then analyzed using a FACSCalibur flow cytometer (BD Biosciences), and data analysis was performed with CellQuest software (BD Biosciences). For the purification of CD3$^-$CD4$^+$CD45$^+$ cells from infant nasal tissues (10-day-old) and embryonic intestines (17-day-old embryos (E17)), we used an AutoMACS (Miltenyi Biotec) combined with a FACSAria cell sorter (BD Biosciences), as described previously (3).

Isolation of NALT anlagen for RT-PCR

Following the manufacturer's recommendations, we obtained RNA from NALT anlagen by using the laser microdissection (LMD) system (Leica Microsystems). Unfixed nasal tissues isolated from newborn, 7-day-old, 14-day-old, and 6-wk-old mice were frozen in liquid nitrogen. Samples were sectioned into 8-μm thicknesses and immediately fixed in 75% ethanol/diethylpyrocarbonate-treated water for 30 s. Sections were counterstained with toluidine blue (Wako Pure Chemical) for 30 s. After the dehydration with ethanol and xylene, the sections were dissected with a LMD system (Leica Microsystems). The site of NALT formation was captured from each tissue and lysed in TRIzol (Invitrogen Life Technologies) for quantitative RT-PCR using the LightCycler system (Roche Diagnostics) (12).

Primers and hybrid probes for real-time RT-PCR

The primers and hybrid probes used for PCR were as follows: the oligonucleotide primers specific for CXCR5 (sense, 5′-TTCTCCACCCAATGTACC-3′; antisense, 5′-AACCTCTGTCGTCATTCTC-3′), CXCR5 detection FITC-labeled probe (5′-ATTCTACGCACCAATGGGGAAGGAAGC CAACT-3′), and LightCycler Red 640-labeled hybrid probe (5′-GCCTGGG GAAAGCAAGATAGCAAAGTGGTCCTA-3′); the oligonucleotide primers specific for CCR7 (sense, 5′-ATGCTGGCTATGAGTTTC-3′; antisense, 5′-GCTGCTATTGGTGATGTT-3′), CCR7 detection FITC-labeled probe (5′-ATGATCACCTTGATGGCCTTGTTCCGCTCAAAG-3′), and LightCycler Red 640-labeled hybrid probe (5′-TGCGTGCCTGGAGCAAGG TACGGATGATAATGA-3′); the oligonucleotide primers specific for CXCL13 (sense, 5′-GAACAGGCATTTAGTGACAAC-3′; antisense, 5′-TTTTGGAAGCCTGCGTTTT-3′), CXCL13 detection FITC-labeled probe (5′-AATGTGAACTTGTAGCTCGTACTAACAAGAGG-3′), and LightCycler Red 640-labeled hybrid probe (5′-TTGCGAGATGGACT TCAGTTATTTTGCACC-3′); the oligonucleotide primers specific for CCL19 (sense, 5′-GCCAAGAACAAAGGCAACA-3′, antisense, 5′-CA CACTCACATCGACTCTCTA-3′), CCL19 detection FITC-labeled probe (5′-TGGCCCAGGAAACCAAGGACCA-3′), and LightCycler Red 640-labeled hybrid probe (5′-AAGAGAGGACCAGGCCTCCT-3′); the oligonucleotide primers specific for CCL21a (sense, 5′-ACAGACACAGCCCTCAA-3′; antisense, 5′-CATGAGGTGGCTGCTTT-3′), CCL21a detection FITC-labeled probe (5′-CCAGGAGATCCCCCACGAACTTC-3′), and LightCycler Red 640-labeled hybrid probe (5′-AGCTGGGTGGT TCACGGT-3′); and the oligonucleotide primers specific for GAPDH (sense, 5′-TGAACGGGAAGCTCACTGG-3′; antisense, 5′-TCCACCACCCT GTTGCTGTA-3′), GAPDH detection FITC-labeled probe (5′-CTGAG GACCAGGTTGTCTCCTGCGA-3′), and LightCycler Red 640-labeled hybrid probe (5′-TTCAACAGCAACTCCCACTCTTCCACC-3′). They were designed and produced by Nihon Gene Research Laboratories.

Immunohistochemistry

For confocal microscopic analysis, the nasal tissues and intestines were fixed in 4% paraformaldehyde for the preparation of cryostat sections (5 μm) (3). These tissues were then stained with appropriate fluorescence-conjugated mAb as described above. To assess the formation of the germinal center and follicular dendritic cell (FDC) network in NALT, the previously described nasal immunization protocol was used (3). NALT sections were incubated with biotinylated peanut agglutinin (PNA) (Vector Laboratories) and then stained with FITC-streptavidin (BD Pharmingen). To detect the FDC network, the serial sections were stained with anti-FDC-M1 (BD Pharmingen) and then visualized with FITC-conjugated anti-rat IgG (BD Pharmingen). Histological analysis was performed using a confocal microscope (Leica Microsystems).

Results and Discussion

Lymphoid chemokine family-independent accumulation of CD3$^-$CD4$^+$CD45$^+$ cells at the NALT anlagen

The lymphoid chemokines CXCL13, CCL19, and CCL21 were shown to be involved in the migration of CD3$^-$CD4$^+$CD45$^+$ inducer cells into the PP anlagen (5, 6). Our previous study showed that CD3$^-$CD4$^+$CD45$^+$ inducer cells accumulated at the site of NALT development in mice aged between 7 and 10 days (3). When these lymphoid chemokine-deficient mice were examined, we detected a cluster of the inducer cells at the site of NALT formation in the infant nasal cavity of 10-day-old CXCL13$^{-/-}$ mice, *plt/plt* mice, and CXCL13$^{-/-}$*plt/plt* mice in addition to 10-day-old C57BL/6 and BALB/c mice (Fig. 1*A*). The size of the CD3$^-$CD4$^+$ inducer cell cluster in the NALT anlagen of CXCL13$^{-/-}$ infant mice and *plt/plt* infant mice was similar to that observed in control C57BL/6 and BALB/c mice, respectively. When single-cell preparations from nasal tissues of 10-day-old CXCL13$^{-/-}$ mice, 10-day-old *plt/plt* mice, and 10-day-old CXCL13$^{-/-}$*plt/plt* infant mice were examined, CD3$^-$CD4$^+$CD45$^+$ cells were also found (Fig. 2*A*). The number of CD3$^-$CD4$^+$CD45$^+$ cells isolated from nasal tissues of CXCL13$^{-/-}$ mice, *plt/plt* mice, and CXCL13$^{-/-}$*plt/plt* mice did not differ significantly from that of controls (Fig. 2*B*). As one might expect based on the previous study (6), several cellular clusters of CD3$^-$CD4$^+$ inducer cells were observed in the intestine of 17-day-old embryos (E17) of C57BL/6 and BALB/c mice (Fig. 1*B*). In contrast, we could not detect any signs of an accumulation of CD3$^-$CD4$^+$ inducer cells in intestines isolated from E17 CXCL13$^{-/-}$ mice and CXCL13$^{-/-}$*plt/plt* mice (Fig. 1*B*). These results confirm those of a previous study (6) and indicate that the degree to which the initiation of tissue genesis depends on lymphoid chemokines can be used to distinguish NALT inducer cells (NALTi) (independent) from PP inducer cells (PPi) (dependent). Thus, CXCL13 is indispensable for the accumulation of CD3$^-$CD4$^+$CD45$^+$ PPi but not of NALTi in the respective tissue anlagen.

Unexpectedly, the accumulation of inducer cells was also observed in the mesentery of E17 CXCL13$^{-/-}$ mice and CXCL13$^{-/-}$*plt/plt* mice, indicating that CXCL13 is not essential for the formation of mesenteric LN (MLN), the other member of GALT (Fig. 1*C*). Furthermore, the development of MLN was conserved in CXCR5$^{-/-}$ mice and CXCR5$^{-/-}$CCR7$^{-/-}$ mice (7). Even among GALT, then, the migration of CD3$^-$CD4$^+$ cells into the specific tissue anlagen (e.g., PP and MLN) shows a variable dependence on CXCL13. Surprisingly, FACS analysis revealed that CD3$^-$CD4$^+$CD45$^+$ cells were observed in mononuclear cells isolated from E17 intestines of CXCL13$^{-/-}$ mice, *plt/plt* mice, and CXCL13$^{-/-}$*plt/plt* mice (Fig. 2*A*). The number and the

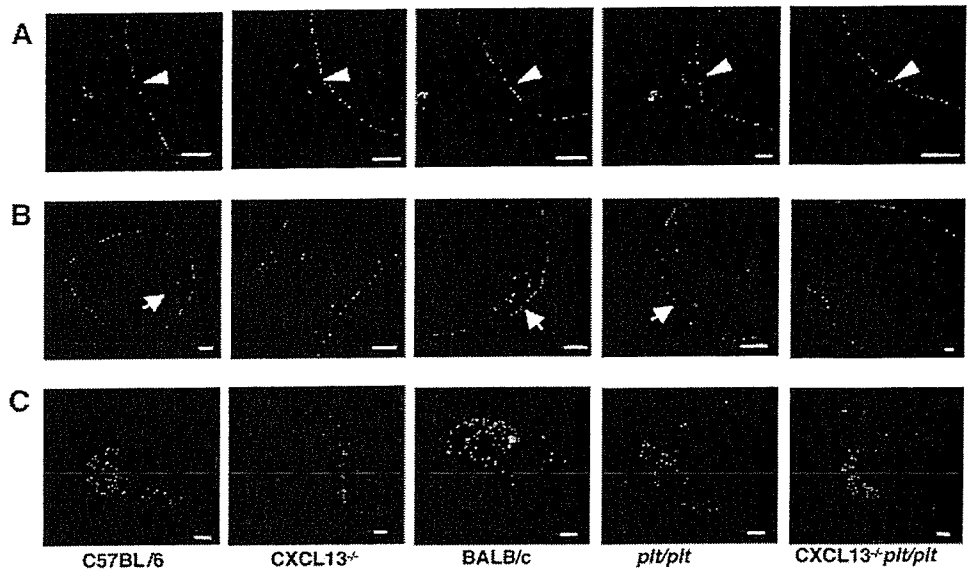

FIGURE 1. Histological analysis of infant nasal tissues and fetal intestines in lymphoid chemokine-null mice. *A*, Nasal tissues were isolated from 10-day-old C57BL/6, $CXCL13^{-/-}$, BALB/c, *plt/plt*, and $CXCL13^{-/-}$*plt/plt* mice. *B*, Fetal intestine was isolated from E17 of C57BL/6, $CXCL13^{-/-}$, BALB/c, *plt/plt*, and $CXCL13^{-/-}$*plt/plt* mice. *C*, Mesenteries were isolated from E17 C57BL/6, $CXCL13^{-/-}$, BALB/c, *plt/plt*, and $CXCL13^{-/-}$*plt/plt* mice. Frozen sections were incubated with anti-mouse CD3ε-FITC (green) and anti-mouse CD4-PE (red). Arrowheads in *A* and arrows in *B* indicate the accumulation of $CD3^-CD4^+$ cells at the anlagen of NALT and PP, respectively. Scale of bars, 100 μm.

frequency of $CD3^-CD4^+CD45^+$ cells in $CXCL13^{-/-}$ and *plt/plt* embryonic intestines did not differ significantly from those observed in control mice (Fig. 2). These results indicate that the migration of $CD3^-CD4^+CD45^+$ cells into embryonic intestine does not depend on lymphoid chemokines; however, CXCL13 is essential for directing the inducer cells at the site of PP anlagen.

These data demonstrate that $CD3^-CD4^+CD45^+$ NALTi can migrate to the site of NALT formation without lymphoid chemokines such as CXCL13, CCL19, and CCL21, which are known to be associated with the other lymphoid tissue genesis programs. Furthermore, the size of the $CD3^-CD4^+CD45^+$ cell cluster and the number of $CD3^-CD4^+CD45^+$ cells in infant nasal tissues did not change in lymphoid chemokine-deficient mice. Thus, the PP genesis-associated lymphoid chemokines may not have any involvement in the formation of the NALT anlagen operated by the NALTi. If that is the case, then our efforts should be focused on identifying the molecules that are at work in the migration of NALTi to the NALT anlagen.

The expression of chemokine receptors by NALTi

Inasmuch as the chemokine receptor family of CXCR5 and CCR7 has been shown to play a key role in the migration of PPi to the tissue genesis site (5), it was logical to next examine the use of the chemokines by NALTi. We first performed quantitative RT-PCR to examine the levels of CXCR5 and CCR7 expression by NALTi and PPi. For both chemokine receptors, levels expressed by NALTi were significantly lower than those expressed by PPi (Fig. 3*A*). Thus, CXCR5 and CCR7 expression by NALTi fell to levels that were barely detectable. The finding was further confirmed by FACS analysis, where PPi expressed CXCR5 and CCR7, especially the $CD4^{high}$ fraction (Fig. 3*B*). However, NALTi expressed neither CXCR5 nor CCR7 (Fig. 3*B*).

The interaction of CXCR5/CXCL13 essentially promotes chemotactic activity for the clustering of PPi in the embryonic intestine (5). Furthermore, together with IL-7Rα signaling, CXCR5 is involved in the induction of $LT\alpha1\beta2$ expression on PPi (7). In addition, CXCR5 signaling mediates the activation of β_1 integrin expressed on PPi for the interaction of VCAM-1^+ICAM-1^+ stromal cells at the PP anlagen (6). Although the multipotent function of CXCR5 expressed by PPi is required to initiate the development of PP, NALTi did not express CXCR5. Therefore, NALTi is thought to mediate the initiation of NALT organogenesis without a CXCR5/CXCL13-mediated signal. Furthermore, CCR7 expressed on $CD3^-CD4^+CD45^+$ cells are cooperatively involved in the organogenesis of PP and other LN (5, 7). Given that neither CCR7 nor CXCR5 is expressed on NALTi (Fig. 3, *A* and *B*), it is likely that the initial step of NALT organogenesis is completely independent of the lymphoid chemokine signaling mediated by the corresponding receptors of CXCR5 and CCR7.

Uniqueness in the production of lymphoid chemokines by NALT

To further support our findings using immunohistological analysis of the lymphoid tissue genesis in lymphoid chemokine-deficient mice, CXCL13-specific mRNA was rarely produced at the site of NALT formation of newborn and 7-day-old BALB/c and C57BL/6 mice (Fig. 3*C*). Likewise, the production of CCL19-specific mRNA at NALT anlagen was nil or extremely low in newborn mice. In contrast, we detected constitutive mRNA expression of CCL21 at the site of NALT development in mice newly born up to mice aged 6 wk (Fig. 3*C*). High levels of mRNA expression for CXCL13, CCL19, and CCL21 were also detected in the NALT of 6-wk-old mice (Fig. 3*C*). As NALT developed, the expression of lymphoid chemokines, including CXCL13 and CCL19, gradually increased.

CXCL13 and CCL19 have been shown to be produced by VCAM-1^+ICAM-1^+ stromal cells in the anlagen of PP (5). LTβR signaling through the alternative NF-κB pathway by the interaction of stromal cells and PPi is thought to induce CXCL13, CCL19, and CCL21 expression (2). In the case of NALT, neither CXCL13 nor CCL19 was expressed at birth, but the expression of both gradually increased as NALT matured. Thus, it is interesting to postulate that the initial triggering of CXCL13 and CCL19 production is induced by the cluster of NALTi accumulated at the NALT anlagen in the neonatal stage, with lymphoid cells gradually taking over the expression of these two chemokines.

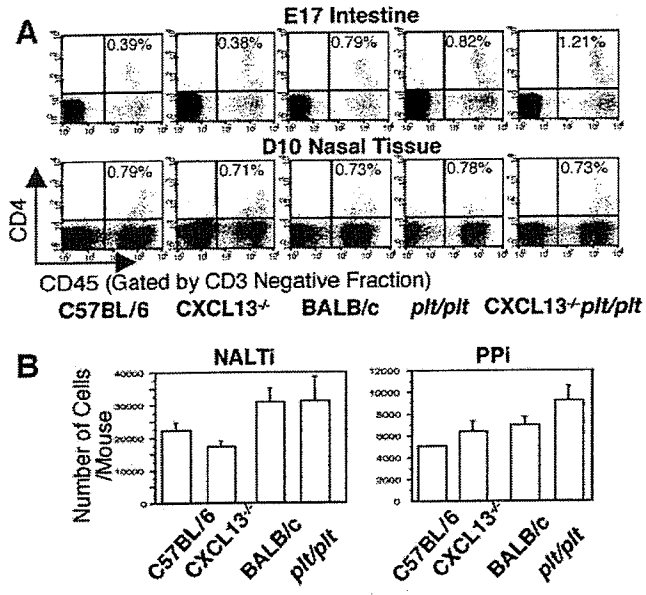

FIGURE 2. Analysis of inducer cells of lymphoid chemokine-null mice. Mononuclear cells were isolated from nasal tissues of 10-day-old mice and intestines of E17 mice. *A*, FACS analysis was performed to detect $CD3^-CD4^+CD45^+$ cells in C57BL/6, $CXCL13^{-/-}$, BALB/c, *plt/plt*, and $CXCL13^{-/-}$*plt/plt* mice. Results are representative of three independent experiments. *B*, The number of $CD3^-CD4^+CD45^+$ cells in day 10 (D10) nasal tissues (NALTi) and E17 intestines (PPi) in C57BL/6, $CXCL13^{-/-}$, BALB/c, and *plt/plt* mice. No significant differences were noted between lymphoid chemokine-null ($CXCL13^{-/-}$ and *plt/plt* mice) and control (C57BL/6 and BALB/c) mice. Significance was evaluated by an unpaired *t* test.

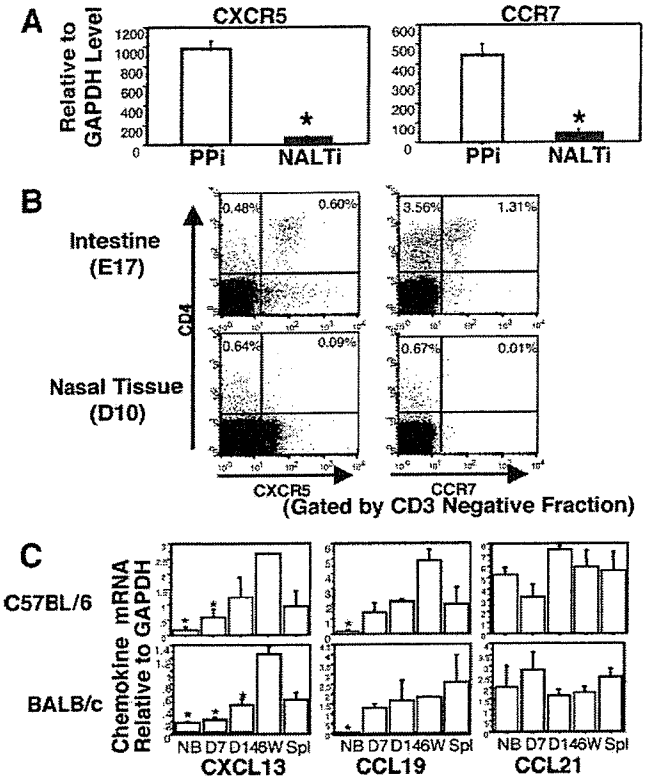

FIGURE 3. Analysis of the expressions of lymphoid chemokines and their corresponding receptors by NALTi and PPi and NALT anlagen. *A*, $CD3^-CD4^+CD45^+$ cells were sorted from mononuclear cells of day 10 (D10) nasal tissues (NALTi) and of E17 intestines (PPi) by FACSAria. Quantitative analysis of CXCR5 and CCL7 mRNA expression was performed using LightCycler. The expression of each chemokine receptor was normalized to the expression of GAPDH. RNA was extracted from three individual experiments per group. Significance was evaluated by an unpaired *t* test. *, $p < 0.05$. *B*, CXCR5 and CCR7 expression of $CD3^-CD4^+$ cells of D10 nasal tissues and E17 intestines were analyzed using FACSCalibur. *C*, Chronological analysis of lymphoid chemokine expression in NALT was performed using NALT anlagen of newborn (NB), 7-day-old (D7), and 14-day-old (D14) mice, NALT, and spleen of 6-wk-old (6W) C57BL/6 and BALB/c mice, which were isolated by a LMD system. Quantitative analysis of mRNA expression of lymphoid chemokines (CXCL13, CCL19, and CCL21) was performed using LightCycler. *, $p < 0.05$ compared with 6 wk via an unpaired *t* test ($n = 3$ on each time point).

CCL21 is produced by stromal cells in the T cell area, endothelial cells of high endothelial venules, and lymphatic vessels (7). Therefore, since the level of CCL21 expression is high at birth and remains high during the maturation stage related to the other two chemokines, stromal cells and endothelial cells in NALT, including anlagen and adult stages, seem to be a key source for the production of CCL21.

Microarchitecture of NALT in the lymphoid chemokine-null mice

Thus far, our data have demonstrated that the lymphoid chemokines CXCL13, CCL19, and CCL21 are not involved in the induction of NALT organogenesis. The role of lymphoid chemokines for the maintenance of mature NALT in adult mice should be investigated next. The total number of mononuclear cells in NALT of young adult $CXCL13^{-/-}$ mice and *plt/plt* mice was always lower than in normal mice (Fig. 4*A*). Of the various lymphoid cell subsets, the population of $B220^+$ B cell saw the greatest decrease, followed by $CD3^+$ cells and $CD11c^+$ cells in the NALT of $CXCL13^{-/-}$ mice (Fig. 4*A*). Furthermore, we sought to determine whether the migration of B1 and B2 cells into NALT might be altered in $CXCL13^{-/-}$ mice since the most obvious alteration was associated with the B cell subset. The level of CXCR5 expression by B1 cells in NALT was similar to that by B2 cells (our unpublished data). Although it has been established that a major subset of NALT B cells belong to B2 cells (13), both B1 and B2 cells were reduced in the NALT of $CXCL13^{-/-}$ mice (our unpublished data). These data indicate that CXCL13 is required for the migration of both B1 and B2 cells into NALT. Using confocal microscopic analysis, we further showed that the microarchitecture of the B cell area was destroyed in $CXCL13^{-/-}$ mice, leaving the NALT extensively occupied by T cells (Fig. 4*B*). The formation of a germinal center and FDC network was thus disrupted in the NALT of $CXCL13^{-/-}$ mice (Fig. 4*B*). In contrast, the T cell area was not observed in the NALT of *plt/plt* mice (Fig. 4*B*). The formation of the germinal center and the FDC network was intact in the NALT of *plt/plt* mice (Fig. 4*B*). These findings suggest that CXCL13 is involved in the recruitment of lymphocytes into NALT instead of the initiation of NALT tissue genesis. Furthermore, it was previously suggested that CXCL13 contributed to the subsequent microarchitecture formation of the B cell zone in NALT (9). However, it should be noted that B cell themselves are also capable of regulating the microarchitecture formation via the use of LT family-mediated signals (8). $LT\alpha1\beta2$-expressing B cells themselves promote the formation of follicles in secondary lymphoid organs (8). Therefore, B cell migration into NALT may also affect the disorganized follicles in the NALT of $CXCL13^{-/-}$ mice. In contrast, CCL19 and CCL21 preferentially promoted T cell migration into NALT

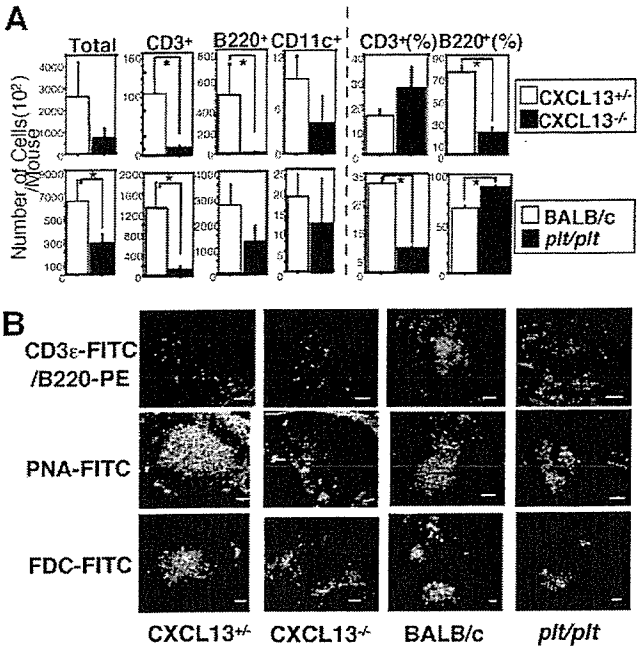

FIGURE 4. Microarchitecture of NALT in adult CXCL13$^{-/-}$ and *plt/plt* mice. *A*, Mononuclear cells isolated from the NALT of CXCL13$^{+/-}$, CXCL13$^{-/-}$, BALB/c, and *plt/plt* mice were analyzed using FACSCalibur. Data were obtained from three individual experiments. Significance was evaluated by an unpaired *t* test. *, $p < 0.05$. *B*, NALT was obtained from CXCL13$^{+/-}$, CXCL13$^{-/-}$, BALB/c, and *plt/plt* mice nasally immunized with cholera toxin. Frozen sections of NALT were incubated with anti-mouse CD3ε-FITC (green) and anti-mouse B220-PE (red) (*top panels*). The formation of a germinal center was analyzed by PNA-FITC (green) (*middle panels*). The network of FDC was stained by anti-FDC-FITC (green) (*bottom panels*). Scale of bars, 80 μm.

but were not involved in the genesis of tissue or the formation of microarchitecture like the germinal center and FDC network.

The cytokine signaling via LTβR induces the expression of CXCL13 by stromal cells in the B cell area for the recruitment of B cells into the follicular regions and the formation of germinal centers in spleen (7). This evidence provides a logical explanation as to why the microarchitecture of NALT is disorganized in mice lacking LTβR signaling (e.g., LTα$^{-/-}$ mice, LTβ$^{-/-}$ mice, and IκB kinase^{AA} mice) (3, 4, 14). Our data further support the findings by Ying et al. (15), which showed that the reduced production of CXCL13, CCL19, and CCL21 in LTα and LTβ deficiency resulted in the disorganization of NALT. Thus, not only do our results confirm the findings that CXCL13 is involved in the maintenance of the microarchitecture of NALT (9) (Fig. 4), they further show that it is not involved in the initiation of the tissue genesis (Figs. 1–3). The analysis of *plt/plt* mice showed that CCL19 and CCL21 promote T cell migration to NALT. CXCL13 also plays an essential role in the formation of the germinal center and FDC network, whereas CCL19 and CCL21 are not involved.

Our findings demonstrate that the lymphoid chemokine family interactions of CXCR5/CXCL13 and CCR7/CCL19 and CCL21 are not essential for the initiation of NALT genesis associated with the NALTi migration into the NALT anlagen. However, as our current study demonstrates, these lymphoid chemokines do play key roles in the creation and maintenance of NALT structure in adult mice. The latter finding is in total agreement with the recent study by Rangel-Monero et al. (9), which showed CXCL13, CCL19, and CCL21 were required for the organization of NALT. Our further examinations suggested that the lymphoid chemokine interactions of CXCR5/CXCL13 and CCR7/CCL19 and CCL21 provide distinct signals for the initiation of tissue genesis, as well as recruitment of lymphoid cells and subsequent microarchitecture formation of different mucosa-associated lymphoid tissues located in the aero-digestive tract.

Acknowledgments

We thank Dr. H. Nakano in the Department of Medicine and Division of Cardiology, Duke University Medical Center, for technical advice on mating *plt/plt* mice. We also thank the members of our laboratory for their technical advice and helpful discussions.

Disclosures

The authors have no financial conflict of interest.

References

1. Kiyono, H., and S. Fukuyama. 2004. NALT- versus Peyer's-patch-mediated mucosal immunity. *Nat. Rev. Immunol.* 4: 699–710.
2. Mebius, R. E. 2003. Organogenesis of lymphoid tissues. *Nat. Rev. Immunol.* 3: 292–303.
3. Fukuyama, S., T. Hiroi, Y. Yokota, P. D. Rennert, M. Yanagita, N. Kinoshita, S. Terawaki, T. Shikina, M. Yamamoto, Y. Kurono, and H. Kiyono. 2002. Initiation of NALT organogenesis is independent of the IL-7R, LTβR, and NIK signaling pathways but requires the *Id2* gene and CD3$^-$CD4$^+$CD45$^+$ cells. *Immunity* 17: 31–40.
4. Harmsen, A., K. Kusser, L. Hartson, M. Tighe, M. J. Sunshine, J. D. Sedgwick, Y. Choi, D. R. Littman, and T. D. Randall. 2002. Cutting edge: organogenesis of nasal-associated lymphoid tissue (NALT) occurs independently of lymphotoxin-α (LTα) and retinoic acid receptor-related orphan receptor-γ, but the organization of NALT is LTα dependent. *J. Immunol.* 168: 986–990.
5. Honda, K., H. Nakano, H. Yoshida, S. Nishikawa, P. Rennert, K. Ikuta, M. Tamechika, K. Yamaguchi, T. Fukumoto, T. Chiba, and S. I. Nishikawa. 2001. Molecular basis for hematopoietic/mesenchymal interaction during initiation of Peyer's patch organogenesis. *J. Exp. Med.* 193: 621–630.
6. Finke, D., H. Acha-Orbea, A. Mattis, M. Lipp, and J. Kraehenbuhl. 2002. CD4$^+$CD3$^-$ cells induce Peyer's patch development: role of $\alpha_4\beta_1$ integrin activation by CXCR5. *Immunity* 17: 363–373.
7. Muller, G., U. E. Hopken, and M. Lipp. 2003. The impact of CCR7 and CXCR5 on lymphoid organ development and systemic immunity. *Immunol. Rev.* 195: 117–135.
8. Cyster, J. G. 2003. Lymphoid organ development and cell migration. *Immunol. Rev.* 195: 5–14.
9. Rangel-Moreno, J., J. Moyron-Quiroz, K. Kusser, L. Hartson, H. Nakano, and T. D. Randall. 2005. Role of CXC chemokine ligand 13, CC chemokine ligand (CCL)19, and CCL21 in the organization and function of nasal-associated lymphoid tissue. *J. Immunol.* 175: 4904–4913.
10. Ebisuno, Y., T. Tanaka, N. Kanemitsu, H. Kanda, K. Yamaguchi, T. Kaisho, S. Akira, and M. Miyasaka. 2003. Cutting edge: the B cell chemokine CXC chemokine ligand 13/B lymphocyte chemoattractant is expressed in the high endothelial venules of lymph nodes and Peyer's patches and affects B cell trafficking across high endothelial venules. *J. Immunol.* 171: 1642–1646.
11. Nakano, H., S. Mori, H. Yonekawa, H. Nariuchi, A. Matsuzawa, and T. Kakiuchi. 1998. A novel mutant gene involved in T lymphocyte-specific homing into peripheral lymphoid organs on mouse chromosome 4. *Blood* 91: 2886–2895.
12. Kinoshita, N., T. Hiroi, N. Ohta, S. Fukuyama, E. J. Park, and H. Kiyono. 2002. Autocrine IL-15 mediates intestinal epithelial cell death via the activation of neighboring intraepithelial NK cells. *J. Immunol.* 169: 6187–6192.
13. Hiroi, T., M. Yanagita, H. Iijima, K. Iwatani, T. Yoshida, K. Takatsu, and H. Kiyono. 1999. Deficiency of IL-5 receptor α-chain selectively influences the development of the common mucosal immune system independent IgA-producing B-1 cell in mucosa-associated tissues. *J. Immunol.* 162: 821–828.
14. Drayton, D. L., G. Bonizzi, X. Ying, S. Liao, M. Karin, and N. H. Ruddle. 2004. IκB kinase complex α kinase activity controls chemokine and high endothelial venule gene expression in lymph nodes and nasal-associated lymphoid tissue. *J. Immunol.* 173: 6161–6168.
15. Ying, X., K. Chan, P. Shenoy, M. Hill, and N. H. Ruddle. 2005. Lymphotoxin plays a crucial role in the development and function of nasal-associated lymphoid tissue through regulation of chemokines and peripheral node addressin. *Am. J. Pathol.* 166: 135–146.

A Second Generation of Double Mutant Cholera Toxin Adjuvants: Enhanced Immunity without Intracellular Trafficking[1]

Yukari Hagiwara,*† Yuki I. Kawamura,‡ Kosuke Kataoka,* Bibi Rahima,* Raymond J. Jackson,* Katsuhiro Komase,† Taeko Dohi,‡ Prosper N. Boyaka,* Yoshifumi Takeda,§ Hiroshi Kiyono,*¶ Jerry R. McGhee,* and Kohtaro Fujihashi[2]*

Nasal application of native cholera toxin (nCT) as a mucosal adjuvant has potential toxicity for the CNS through binding to GM1 gangliosides in the olfactory nerves. Although mutants of cholera toxin (mCTs) have been developed that show mucosal adjuvant activity without toxicity, it still remains unclear whether these mCTs will induce CNS damage. To help overcome these concerns, in this study we created new double mutant CTs (dmCTs) that have two amino acid substitutions in the ADP-ribosyltransferase active center (E112K) and COOH-terminal KDEL (E112K/KDEV or E112K/KDGL). Confocal microscopic analysis showed that intracellular localization of dmCTs differed from that of mCTs and nCTs in intestinal epithelial T84 cells. Furthermore, both dmCTs exhibited very low toxicity in the Y1 cell assay and mouse ileal loop tests. When mucosal adjuvanticity was examined, both dmCTs induced enhanced OVA-specific immune responses in both mucosal and systemic lymphoid tissues. Interestingly, although both dmCT E112K/KDEV and dmCT E112K/KDGL showed high Th2-type and significant Th1-type cytokine responses by OVA-specific CD4$^+$ T cells, dmCT E112K/KDEV exhibited significantly lower Th1-type cytokine responses than did nCT and dmCT E112K/KDGL. These results show that newly developed dmCTs retain strong biological adjuvant activity without CNS toxicity. *The Journal of Immunology,* **2006, 177: 3045–3054.**

An important aspect of immune responses at mucosal surfaces is the production of polymeric IgA Abs, as well as their transport across the epithelium and release as secretory IgA (S-IgA).[3] Because this S-IgA Ab response represents the first major line of defense against invasion by viral and bacterial pathogens (1), recent efforts have been focused on the development of vaccines that are capable of inducing effective immune responses in mucosal tissues. However, most protein Ags are rather weak immunogens when given by a mucosal route. If the full potential of the new generation of mucosal vaccines is to be realized, effective and reliable mucosal adjuvants must be developed.

Our recent study (2) showed that nasal vaccines for nasopharyngeal-associated lymphoreticular tissue (NALT)-based mucosal immunity could make a significant contribution to protecting the elderly. Furthermore, these nasal and oral vaccines would be easier to administer than parenteral ones. Mucosal vaccines would also carry less risk of transmitting infections like hepatitis B and HIV, which are still associated with the use of injectable vaccines in several parts of the world. Despite these many attractive features, it has often proved difficult in practice to stimulate strong mucosal S-IgA Ab responses with subsequent protection by the use of mucosal administration of vaccines, and the results to date for mucosal vaccinations using soluble protein Ags have been, with a few notable exceptions, rather disappointing (3).

Native cholera toxin (nCT) produced by *Vibrio cholerae* is structurally similar to the native heat-labile enterotoxin (nLT) of enterotoxigenic *Escherichia coli*. Both toxins act as adjuvants for the enhancement of mucosal and systemic Ab responses to coadministered protein Ags given by either oral or nasal routes (4–7) and, consequently, are the most widely used experimental mucosal adjuvants in animal models. Furthermore, both act as mucosal adjuvants by inducing CD4$^+$ Th2 cells secreting IL-4, IL-5, IL-6, and IL-10, which provide help for Ag-specific S-IgA as well as plasma IgG1, IgA, and IgE Ab responses (8, 9). Although they are potent mucosal adjuvants, both nCT and nLT are also toxic and, thus, are not suitable for use with mucosal vaccines in humans. Therefore, a number of nontoxic mutant derivatives of cholera toxin (CT) or heat-labile enterotoxin (LT) have been constructed.

Our own group has contributed to the efforts of constructing nontoxic mutant derivatives; we generated two mutant CTs (mCTs), mCT S61F and mCT E112K, by substituting a single amino acid in the ADP-ribosyltransferase active center of the A

*Departments of Pediatric Dentistry and Microbiology, Immunobiology Vaccine Center, University of Alabama at Birmingham, Birmingham, AL 35294; †Research Center for Biologicals, Kitasato Institute, Saitama, Japan; ‡Department of Gastroenterology, Research Institute, International Medical Center of Japan, Tokyo, Japan; §Cine-Science Laboratory Co. Ltd., Tokyo, Japan; and ¶Division of Mucosal Immunology, Department of Microbiology and Immunology, Institute of Medical Science, University of Tokyo, Tokyo, Japan

Received for publication September 27, 2005. Accepted for publication June 10, 2006.

The costs of publication of this article were defrayed in part by the payment of page charges. This article must therefore be hereby marked *advertisement* in accordance with 18 U.S.C. Section 1734 solely to indicate this fact.

[1] This research was supported by National Institutes of Health Grants DC 04976, DE 12242, AI 18958, and AI 43197 and Grants-in-Aid from the Ministry of Health and Labor, Japan, the Ministry of Education, Science and Sports, Japan, and CREST of Japan Science and Technology Corporation.

[2] Address correspondence and reprint requests to Dr. Kohtaro Fujihashi, Department of Pediatric Dentistry, Immunobiology Vaccine Center, University of Alabama at Birmingham, 761 Bevill Biomedical Research Building, 845 19th Street South, Birmingham, AL 35294-2170. E-mail address: kohtarof@uab.edu

[3] Abbreviations used in this paper: S-IgA, secretory IgA; AFC, Ab forming cell; CHO, Chinese hamster ovary; CLN, cervical lymph node; CT, cholera toxin; nCT, native CT; CT-A, A subunit of nCT; CT-B, B subunit of nCT; dmCT, double mutant CT; mCT, mutant CT; DD, dimer of an Ig binding element; ER, endoplasmic reticulum; LT, heat-labile enterotoxin; nLT, native LT; NALT, nasopharyngeal-associated lymphoreticular tissue; NP, nasal passage; OB, olfactory bulb; ON/E, olfactory nerves and epithelium; SMG, submandibular gland.

Copyright © 2006 by The American Association of Immunologists, Inc.

0022-1767/06/$02.00

subunit (10, 11). Although these originally created forms of mCT did not induce ADP-ribosylation and cAMP formation, they still served as mucosal adjuvants by inducing $CD4^+$ Th2 cells, thereby providing effective help for Ag-specific, mucosal S-IgA, as well as plasma IgG and IgA Ab responses.

It is clearly too dangerous to use an enterotoxin as an adjuvant for mucosal vaccines in humans. Our previous studies have shown that nasally administered nCT accumulates in the olfactory nerves and epithelium (ON/E) and olfactory bulbs (OBs) of mice after binding to GM1 gangliosides (12). Furthermore, nCT as a mucosal adjuvant redirects coadministered protein Ags into these neuronal tissues (12). This finding has provoked some concern about the potential role for ganglioside GM1-binding molecules that target neuronal tissues, including the CNS, in nasal immunization. Although deposition of nCT via the ON/E and OBs did not lead to obvious pathologic changes in brain tissue after nasal administration (13), it has been reported that a human vaccine containing inactivated influenza and nLT as an adjuvant resulted in a very high incidence of Bell's palsy (14, 15). These results strongly indicate that it is essential to develop a safer and more effective nasal adjuvant for human use.

Both nCT and nLT consist of a ring of five B subunits and a single A subunit that is cleaved into A1 and A2 chains. Previous studies showed that the carboxyl terminus of the A2 subunit of nCT contains the ER retention signal tetrapeptide KDEL (RDEL in LT). These results show that the toxin is transported via the vesicles from the plasma membrane to the Golgi compartment with subsequent separation of the A and B subunits of nCT (designated throughout as CT-A and CT-B, respectively). The CT-A subunit is redirected to the plasma membrane by retrograde transport via the ER, whereas the CT-B subunit persists in the Golgi compartment. The intracellular target of toxin is G_s, the stimulatory regulatory component of adenyl cyclase (16, 17). Thus, mutations in KDEL influence the movement of CT from the Golgi apparatus to the ER (18–21). It has previously been shown that mutation in K(R)DEL of both CT and LT delayed the time course of toxin-induced Cl^- secretion. Furthermore, consistent with a slower rate of signal transduction, KDEL mutants trafficked more slowly to the basolateral membrane than did nCT (18, 19).

However, a recent report indicated that mutant LT RDEL retained ADP-ribosyltransferase activity and induced morphological changes in Chinese hamster ovary (CHO) cell cultures (19). In contrast, mCT E112K has proven to be a safe and stable adjuvant (10, 11, 13, 22). The mCT E112K was constructed to be devoid of toxicity while retaining its adjuvant activity. Our previous studies showed that mCT E112K was effective in the murine system. Nasal immunization of OVA, the pneumococcal surface protein A of *Streptococcus pneumoniae*, or diphtheria toxoid plus mCT E112K elicited both Ag-specific IgA and IgG Ab responses in mucosal and systemic immune compartments (10, 11, 13). Although our recent studies showed that mCT E112K did not elicit any neuronal damage based upon nerve growth factor-β1 production in the CNS as well as Ag redirection (23, 24), these studies did not provide any direct information as to whether mCT E112K migrates into the CNS after nasal application. In this regard, we have developed double mutants of CT (dmCTs) by introducing a potent mutation in the ADP-ribosylation activity center and KDEL (E112K/KDEV or E112K/KDGL). Therefore, it is now essential for us to determine whether potentially less trafficking of these new dmCTs, when compared with mCT E112K, will occur in their distribution into the CNS. In this study, we have examined the mucosal adjuvanticity and toxicity of these two dmCTs for our continuing efforts to develop safe and effective nasal adjuvants for mucosal vaccines.

Materials and Methods

Preparation of recombinant mCTs

The plasmids containing nCT or mCT E112K genes were constructed as described previously (10). These plasmids were cloned into pUC119 of a 3.1-kb *EcoRI/PstI* DNA fragment including nCT or mCT E112K genes (10). The KDGL and KDEV mutants were constructed by site-directed mutagenesis in which amino acid substitutions were introduced on a plasmid of nCT using PCR. The following oligonucleotides were used to create genes encoding the mutant toxins KDEV and KDGL: 5′-TAA GGA TGA AGT ATG ATT AAA TTA A-3′ and 5′-TAG AAT TAA GGA TGG ATT ATG ATT A-3′ (mutant codons underlined). To construct dmCT E112K/KDEV and E112K/KDGL, the *BspEI/HincII* fragments including KDEV or KDGL mutations were ligated to a plasmid of mCT E112K. After the DNA sequences were confirmed, pUC119 harboring the mutated CT genes at the *EcoRI/PstI* site were transformed into *E. coli* DH5-α. The *E. coli* strains containing the plasmids for the dmCT genes were grown in Luria-Bertani medium (10 g of NaCl, 10 g of tryptone, and 5 g of yeast extract per liter) with 100 μg/ml ampicillin, and dmCTs were purified according to the method described previously (25). Briefly, the bacteria were harvested and lysed with a sonicator (Insonator 201M; Kubota). The crude lysate was then applied to an immobilized D-galactose column (Pierce) and eluted with galactose. The purified recombinant dmCTs contained <0.05 endotoxin U/μg protein.

Intracellular tracking

Human intestinal epithelial T84 cells were incubated with 10 μg/ml Alexa Fluor 488-conjugated nCT, mCT E112K, dmCT E112K/KDEV, or dmCT E112K/EDGL. To identify their intracellular destination, we used boron dipyrromethane Texas Red ceramide (Invitrogen Life Technologies) as a marker for the Golgi apparatus (26) and ER-Tracker (Invitrogen Life Technologies) Blue-White *p*-xylene-bis-pyridinium bromide as a marker for the ER (27). Boron dipyromethane Texas Red-ceramide was added to individual cultures at a concentration of 5 μM for 10 min before termination of the cultures. Cells were washed once before being further cultured in medium containing 2 μM ER-Tracker for 30 min. After incubation, cells were washed three times with PBS and then fixed with 3.7% formaldehyde in PBS for 10 min at room temperature. After fixation, a Leica TCS SP2-AOBS model confocal microscope or a LMS510 model confocal microscope (Zeiss) was used to visualize the cells. The merged color (yellow) area of each Golgi or ER staining image was picked up using Adobe Photoshop software and converted into a black and white picture. The black area in this black and white picture is based upon the original yellow color and was measured using ImageJ (National Institutes of Health). The condition for picking up the yellow area was saved and applied to all pictures. A monolayer of T84 cells covered most of the dish surface; however, for accuracy, we measured the total pixel area covered with cells in the identical picture using ImageJ software. Thus, each picture covers 12.96 mm^2 of culture surface, which is equal to 262144 pixels. The results were shown as the percentage of yellow color area pixels per the total area pixels covered with cells.

Bioassay and toxicity analysis

We next studied the ability of newly created dmCTs and nCT (List Biological Laboratories) to induce toxic effects on cultured mouse Y-1 adrenal tumor cells, following a previously developed procedure (28). Briefly, serial dilutions of dmCT E112K/KDEV, dmCT E112K/KDGL, mCT E112K, or nCT were added to cultures of Y-1 cells at a density of 5×10^4 cells/well in 0.1 ml of F-10 medium (Invitrogen Life Technologies) containing 15% horse serum and 2.5% FCS and incubated at 37°C with 5% CO_2 for 24 h. Light microscopy was then used to examine cells for morphological changes such as the common "rounding" of cells. The toxin concentration required to initiate the rounding of Y-1 cells was determined. For the cAMP assay, 1.5×10^4 CHO cells in F-10 medium containing 1% FCS were cultured with 100 ng/ml dmCT E112K/KDEV, dmCT E112K/KDGL, mCT E112K, or nCT at 37°C with 5% CO_2 for 18 h. Intracellular cAMP measurement was done with an enzyme immunoassay kit (Amersham Biosciences). The protein amount for some samples was determined with a Coomassie protein assay reagent (Pierce), and the levels of cAMP were expressed as picomoles of cAMP per milligram of protein (10). The mouse ileal loop test was conducted essentially as described previously (29, 30). Briefly, the jejenum was ligated with a piece of cotton thread at a distance of ~3 cm from the pylorus. Immediately after ligation, each loop was injected with 0.1 ml of toxin or PBS (as a control). After 3 h, each loop was hung on a fixed clip and stretched by placing another clip weighing 2 g on the other end of the loop. Then, the length and weight of each loop were